5-2018

A Sensor Based Approach to Analyzing Motion in Medical Applications: AV Fistula Cannulation and Rett Syndrome

Jared J. Wells
Clemson University, jwells2694@aol.com

A SENSOR BASED APPROACH TO ANALYZING MOTION IN MEDICAL APPLICATIONS: AV FISTULA CANNULATION AND RETT SYNDROME

A Thesis
Presented to
the Graduate School of
Clemson University

In Partial Fulfillment
of the Requirements for the Degree
Master of Science
Bioengineering

---

by
Jared J. Wells
May 2018

Accepted by:
Dr. Delphine Dean, Committee Chair
Dr. Joseph Singapogu, Committee Co-Chair
Dr. Brian Dean

ABSTRACT

Sensor based motion analysis is employed to assess frequency, severity and duration of Rett syndrome hand stereotypies as well as soft tissue palpation of an arteriovenous fistula. The only prior quantification of Rett symptoms have been visually in a clinical setting; defining palpation skill is largely unprecedented aside from breast tissue examination. We evaluate various sensors used to track motion, measure electromyography, galvanic skin response, and heart rate. The Leap motion controller is evaluated for the viability of tracking hand palpation. Verification tests are performed for determining the feasibility, accuracy, and precision of each sensor. A static phantom was defined as the two endpoints of each of the six fistulas within the palpation simulator and the accuracy of the Leap Motion was <0.9 cm. The 9 DOF motion sensor, EMG sensor, and heart rate sensor all pass their respective verification tests. The galvanic skin response sensor needs further thought into where the electrodes should be placed for proper readings to ensue. All sensors present acceptable precision and accuracy values within the proposed environment; improvements still need to be made for increased performance. Once resolved and perfected, validation studies should verify the preliminary trends of Rett patients' hand stereotypy quantification and palpation by expert versus novice hemodialysis nurses.

ACKNOWLEDGMENTS

I would like to thank firstly my two principle investigators Dr. Delphine Dean and Dr. Joseph Singapogu for their support and guidance during my time at Clemson University. Dr. Singapogu brought me on to his cannulation simulator project and our relationship grew from there. This project eventually turned in to one of my thesis' projects. We've had many meaningful conversations about the development of his mission and have made great strides in fostering novel research towards improving the care of hemodialysis patients. I am grateful to have been a part of Dr. Singapogu's team and I have learned much under his supervision. Dr. Dean has helped me find my way as a research and developer in the bioengineering field ever since I transferred to Clemson University; she has honed my skillset and put them to good use. When Dr. Dean first asked her husband Dr. Brian Dean if he would consider me for a position in his data intensive computing REU I was not sure what to say. My programming skills at the time were limited and were not my top priority. Dr. Brian Dean took a chance on me and found a sensor-based project where I could further develop my programming and electrical talents. This research has now evolved into the other one of my thesis' projects, the Rett syndrome biometric sleeve. I have found a passion for biosensor applications and want to make medical device development my life's work. I owe this to both Dr. Brian and Delphine Dean. I had little knowledge of sensor-based systems prior to the Rett syndrome project, but Melissa McCollum was able to provide me with the knowledge and tools necessary for developing the sleeve. I would like to thank Melissa for her long hours, hard work and dedication to all of her students' projects and especially my own. I

would also like to thank Dr. Kevin Champaigne as well as Dr. Walter Kauffman for their expertise and continued support of the Rett syndrome sleeve. I would like to thank my parents especially for always believing in me and providing me with the tools I need to become the best person I can be. I love both my parents dearly and will always be indebted to them for their steadfast love and support. Last but not least I would like to thank all of my colleagues for their help with my research. They kept me sane and offered me guidance in more than just school; I consider each and every one of them my friend. There are many more who have helped me along the way and I wish I could thank you each individually for your help. Thank you everyone for your assistance and guidance; I owe who I am today to all of you!

TABLE OF CONTENTS

LIST OF TABLES

LIST OF FIGURES

List of Figures (Continued)

Figure Page

List of Figures (Continued)

Figure Page

List of Figures (Continued)

Figure Page

CHAPTER ONE: A BIOMETRIC APPROACH TO ANALYZING RETT SYNDROME'S ABNORMAL EPISODIC BEHAVIOR

INTRODUCTION

Rett syndrome (RTT) is a postnatal neurodevelopmental disorder that occurs primarily in females.[1] One in approximately 10,000 births suffers from RTT which is produced by a mutation in the X-linked methyl CpG binding protein 2 (MECP2).[2] The disease progression begins with normal growth and development during infancy until six to eighteen months, then there is a noticeable loss of motor control combined with speech impairment. The degradation of motor skills eventually results in apraxia: a motor disorder where there is difficulty in motor planning to perform tasks.[1] Compulsive hand movements such as mouthing, wringing, tapping, and washing are identifiable abnormal, involuntary movements classified as an episode.

Rett syndrome can present with a range of disabling symptoms ranging from mild to severe. The progression and severity of Rett syndrome is determined by the location, type and extent of her mutation and X-inactivation. Therefore, two girls of the same age with the same mutation can express symptoms differently. This makes the treatment of this particular disease unique on a case by case basis.[3]

There is no cure for RTT, so treatment focuses on the management of symptoms and improving quality of life.[3] This includes limiting these previously discussed abnormal episodes so patients may have increased motor control. Drug treatments are still in trials with effectiveness based on physician observation, which is for a limited time and can be error-prone. Pharmaceutical companies need a way to quantify whether the drugs are in fact making an

impact on the patient in a positive way and to what extent. The goal of this project was to develop a wearable device that utilizes sensor fusion to quantify the abnormal episodic behavior of Rett syndrome so that symptomatic events can be further analyzed and broken down in terms of frequency, duration, and severity.

RESEARCH DESIGN AND METHODS

The materials utilized primarily consisted of sensors with their supporting hardware and software. The sensors chosen each were extracting a unique biometric in hope that when combined will provide useful insight into the symptoms of the RTT patient. As can be seen in Figure 1, the sensors were sewn onto a lightweight, incognito compression sleeve made of nylon. The sleeve needed to be lightweight and breathable so it would not interfere with the patient's everyday life; concurrently, the sleeve needed to keep the attached sensors in close proximity to the desired locations along the arm.

Figure 1. Sleeve overview

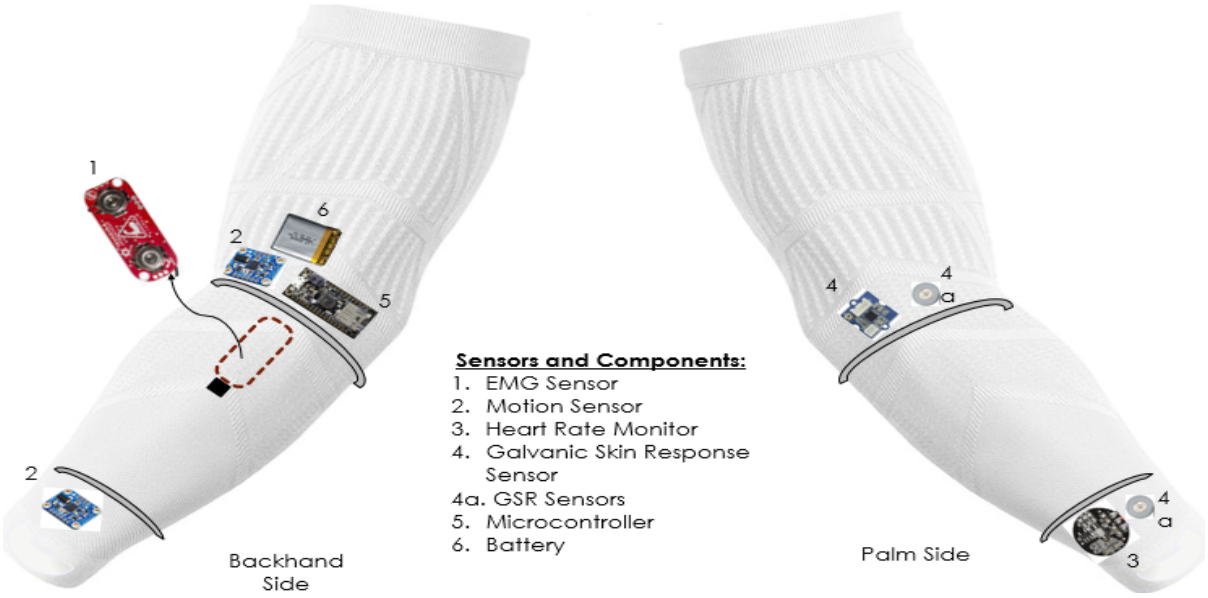

The Feather 32u4 Adalogger produced by Adafruit is the heart of this sensor based device. The Feather which can be seen in Figure 2 is equipped with an ATmega32u4 logic chip running on 3.3 V logic/power at 8 MHz.[4] The built in microUSB, microSD, and battery port allow for easy program uploading, data saving, and battery charging respectively. Because we are recording sensitive patient data we wanted to store the information on an SD card which can be easily given to the patient's presiding physician upon the next visit to the neurology clinic. The Feather is powered by a 500 mAh, 3.7 V lithium ion polymer battery which is more than sufficient to power the sensors we have chosen to run for multiple hours. The I2C, SPI, serial, and analog capabilities of the Feather were of particular interest to us for this project due to some of the sensors outputting a raw analog signal and some outputting a signal for I2C protocol. Briefly, I2C is a serial protocol using only two wires: SCL (serial clock) and SDA (serial data) to connect microcontrollers to peripherals.[5] Each I2C slave device (BNO055, HR, etc…) has a unique 8-bit address that arranges the order of the serial communication with the master device (Feather 32u4 Adalogger). This organizational technique allows for almost unlimited number of I2C slave devices to communicate with the master.[5]

Figure 2. Feather 32u4 Adalogger with battery and SD card components

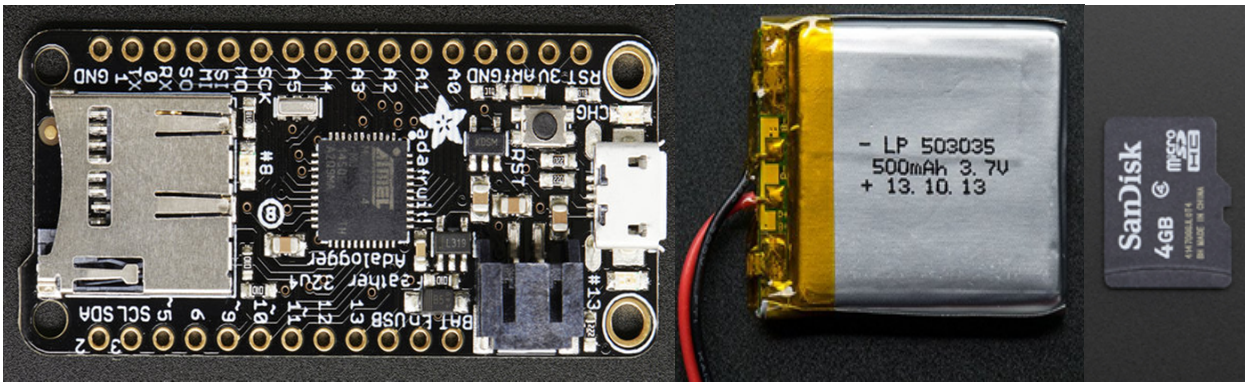

The first sensor we will be discussing is the MyoWare Muscle Sensor by Advancer Technologies. For the reason that Rett syndrome's episodic behavior can usually be identified by a variation of periodic hand motions, it is paramount that our device can record forearm muscle activity as well as hand usage. The MyoWare Muscle Sensor, Figure 3, is able to record electromyography (EMG) which can be directly related to hand or arm activity.[6] An electromyograph detects the electric potential generated by skeletal muscle cells.[7] We chose to place this sensor on the extensor digitorum muscle of the forearm, Figure 5, in hope that the MyoWare will be able to verify the motion captured by the accelerometers and gyroscopes on the elbow and wrist while at the same time recording fine finger movement the motion sensors may not be able to record.

Figure 3. MyoWare Muscle Sensor (.82" x 2.06")

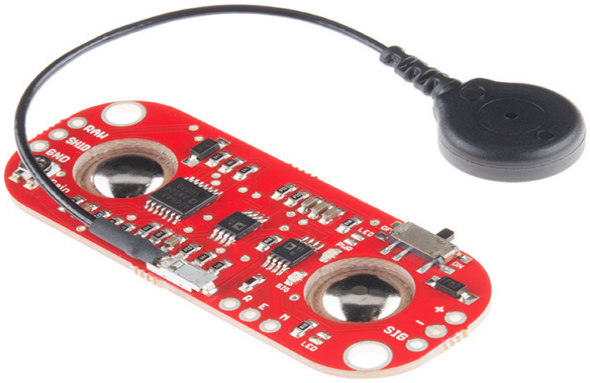

Figure 4. Cognionics Ag/AgCl electrode

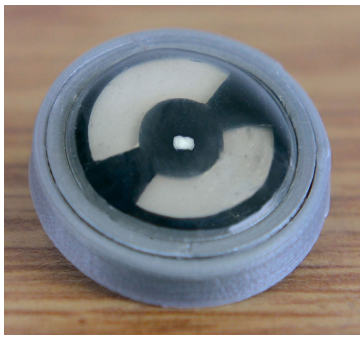

Figure 5. EMG location on forearm along extensor digitorum

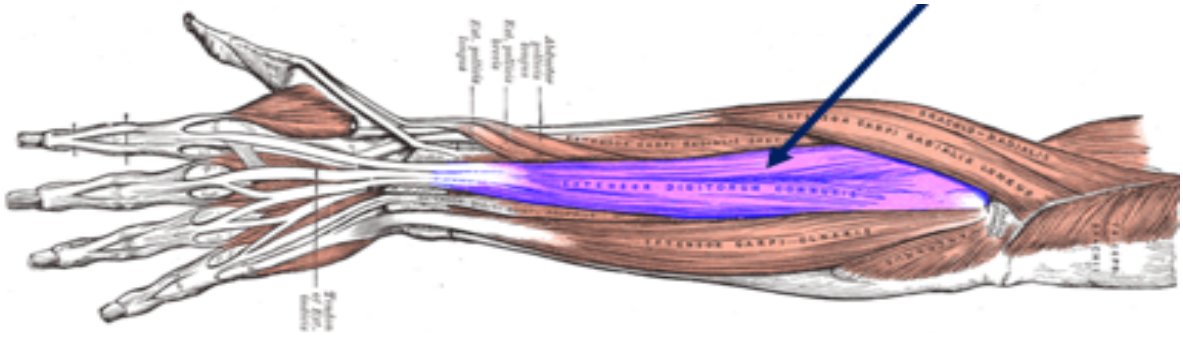

The MyoWare Muscle Sensor requires the use of three separate electrodes: two for which the EMG can be recorded between and one for a reference to an inactive adjacent muscle. The industry standard for electromyography electrodes is the Ag/AgCl wet electrodes. We needed three reusable electrodes that would provide the equivalent level of sensitivity as the industry standard without degradation in signal quality after multiple uses. We chose to use Cognionics' dry, gel electrodes, Figure 4, because they have run numerous comparison tests verifying their dry electrodes are statistically similar to the industry standard which can be seen below in Figure 6.[8] The pad diameter is .67" and easily snaps on to the Myoware Muscle Sensor.

Figure 6. Wet electrodes compared to Cognionics' dry, gel electrodes in response to a stimulus

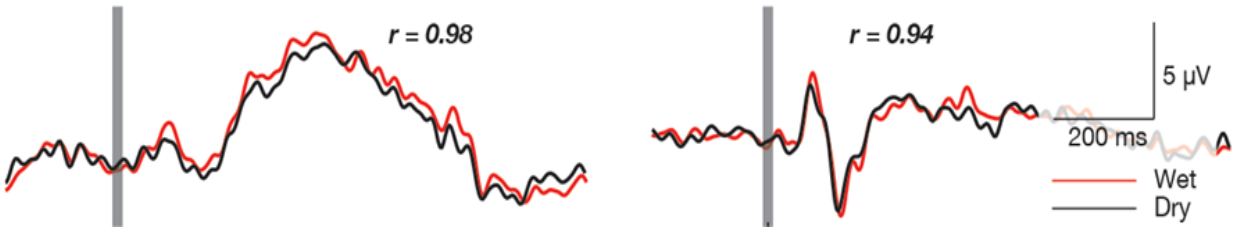

These dry electrodes have a pocket of conductive gel containing an undisclosed combination of salts and electrolytes to act as a transition region for transmitting the electrical activity from under the skin to the Ag/AgCl core.[8] The Ag/AgCl core of these electrodes is what connects to the Myoware Muscle Sensor where the signal can be filtered and then transmitted to the Feather microcontroller via analog signal for data logging.

The second sensor we will be discussing is the BNO055 Absolute Orientation Sensor by Bosch. This sensor will be placed at both the elbow and the wrist as can be seen in the sleeve overview in Figure 1. We decided the motion at the wrist when compared to the elbow would provide novel, more reliable data for better determining the orientation of the patient's arm. The BNO055 is our core motion tracking sensor sized at only 0.15" x 0.21". The BNO055 contains a

32-bit cortex M0+ microcontroller running Bosch Sensortec sensor fusion software which is responsible for providing reliable orientation information in the form of Euler angles (360° sphere). The triaxial 14-bit accelerometer allows us to extract the true linear acceleration vector

Figure 7. BNO055 Absolute Orientation Sensor with axes defined

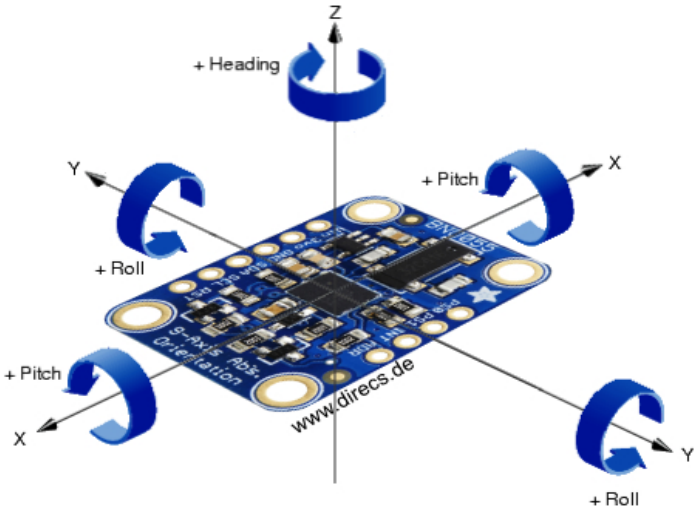

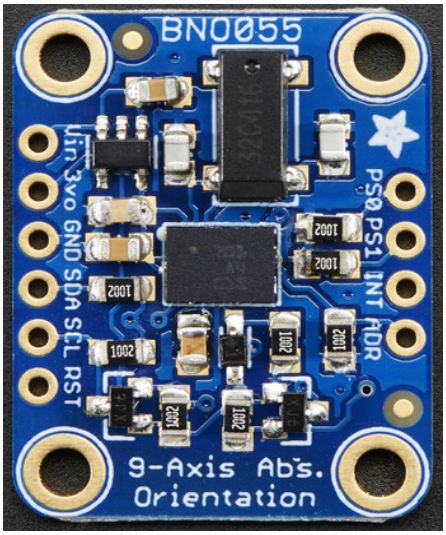

without gravity. The triaxial 16-bit gyroscope has a range of ±2000 degrees per second which permits us to analyze the angular velocity about each individual axis (Figure 7).[9] This is a nine degrees of freedom sensor connected to the Feather microcontroller via I2C protocol.

The third sensor we have attached to our sleeve is the Galvanic Skin Response Sensor (GSR) by Grove Electronics (Figure 8). This sensor is sized at only 0.12” x 0.2”. There are two input electrodes made of nickel that we modified and placed at the proximal and distal ends of the forearm which can be seen in Figure 1 demarked by “Sensor and Component ‘4.’” The GSR sensor measures the resistance between the two electrodes and outputs an analog voltage reading

Figure 8. Galvanic Skin Response Sensor (GSR) by Grove Electronics with two finger electrodes

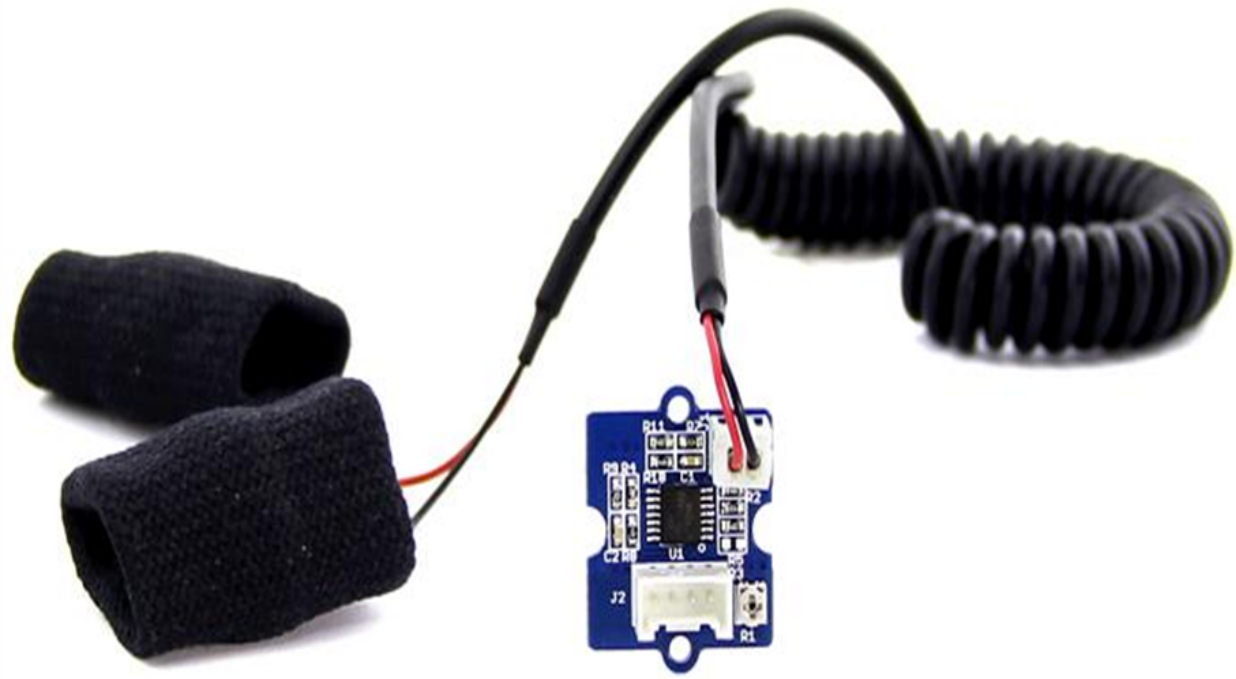

between 0 mV and 1023 mV.[10] We have programmed the GSR sensor to take some readings when the device is first turned on in order to determine the threshold resistance which we can subtract from the subsequent readings. By doing this we are normalizing the GSR readings to 0 so we can more easily see the relative change in resistance. Grove recommends when the two electrodes are placed on the index and middle fingers that a change in voltage of 60 mV or greater is indicative of an emotional response. Galvanic skin response or electrodermal activity is relying on the positive correlation between perspiration and anxiety. Ideally, when someone is feeling more anxious they sweat a little and the GSR sensor picks up on the decrease in resistance between the two electrodes.[10] As we stated before, this change in resistance is conveyed via an analog voltage reading to the Feather microcontroller for further analysis.

The Pulse Sensor Amped by World Famous Electronics is the next sensor we have chosen to utilize. We placed the Pulse Sensor Amped on the exterior of the wrist where one would wear a watch (Figure 1). The Pulse Sensor Amped is only 0.625" in diameter (Figure 9).

Figure 9. Pulse Sensor Amped conveying the emitter, detector, and size

It utilizes photo-plethysmography (PPG) to determine the beats per minute (BPM) of the patient. PPG is used in reflective configuration for the Pulse Sensor Amped meaning the green light-emitting diode (LED) emits light into the tissue and then the reflected light is measured via a detector photodiode on the same side of the tissue.[11] The integrated on board circuitry is a combination of amplifying and filtering circuit components used to measure and smooth the backscatter green light intensity. When the Pulse Sensor Amped is not in contact with any skin the analog signal hovers around the mid-point of the voltage, or V/2. When in close contact with

Figure 10. The red curve represents the pulsed light reflection about V/2 (green line)

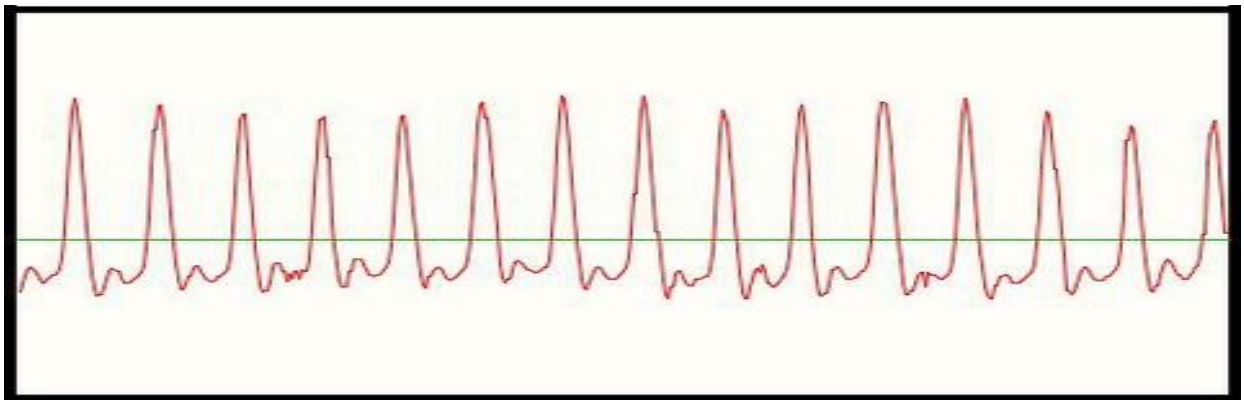

skin, the change in reflected light as blood pumps through the illuminated tissues makes the signal fluctuate around V/2 (Figure 10).[11] The reason for the reflected light intensity fluctuating as a result of the blood pumping through the illuminated tissues is due to the blood volume itself actually fluctuating which can be seen below in Figure 11. To verify the BPM we are recording

Figure 11. Pulse added volume demonstrated

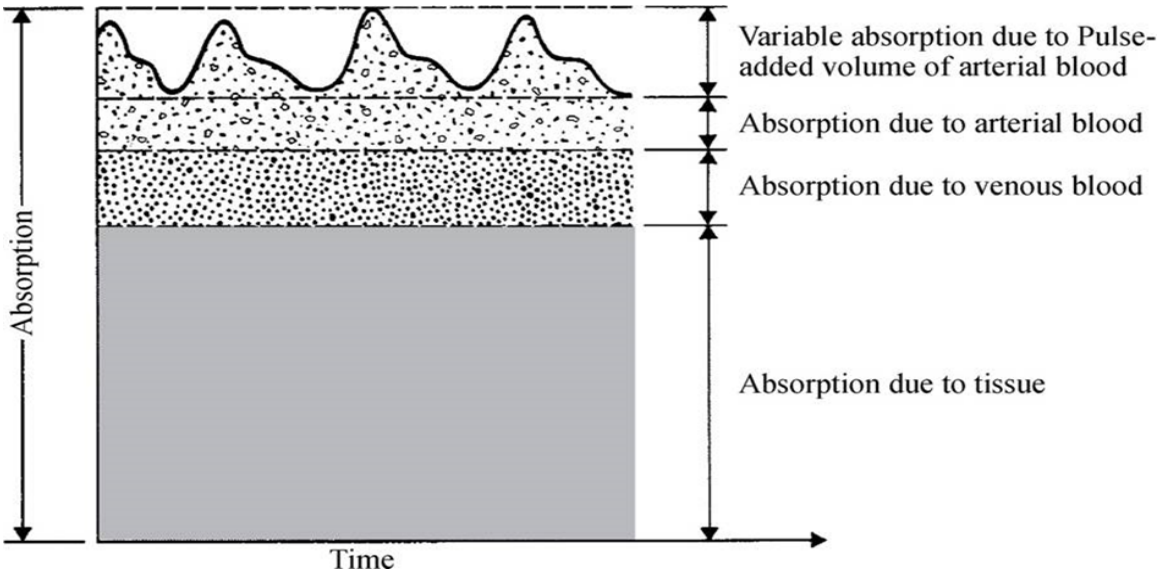

is accurate, we have placed a separate pulse sensor over the radial artery.

The MAX3010 made by Maxim Integrated is only 0.22” x 0.13”. The MAX3010 has the capabilities to record pulse oximetry should this measurement prove to be useful for indicating when a Rett patient is sporadically ventilating. Because of this capability in addition to being able to record the patient’s heart rate, the on-board circuitry has additional ambient light filtering which could prove useful for cleaner BPM readings when outside in sunlight (Figure 12 & 13).[12]

Figure 12. MAX3010 by Maxim Integrated

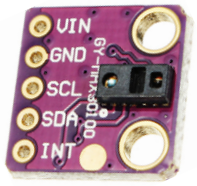

The MAX3010 also utilizes a dim red LED opposed to a bright green LED on the Pulse Sensor Amped.[12] The color of the LED emitter may come in to play under variable lighting conditions.

Figure 13. MAX 3010 block diagram describing signal acquisition and filtering of PPG

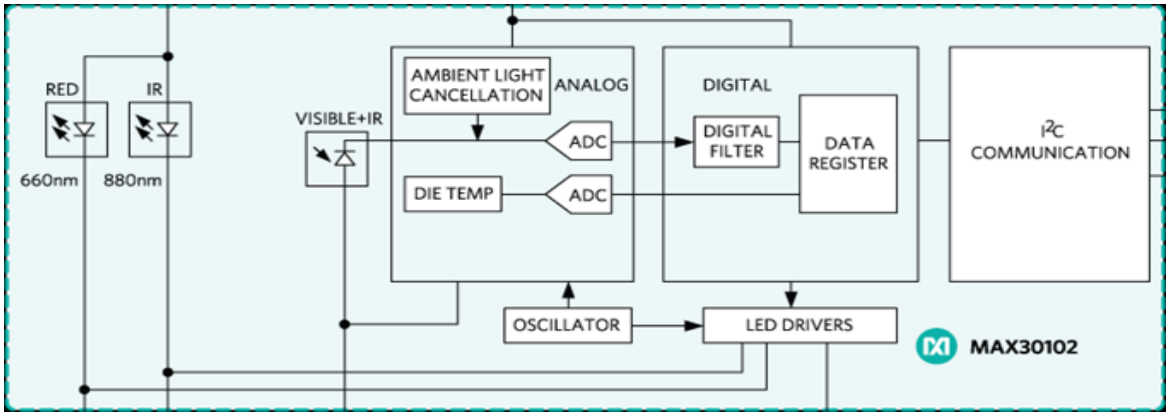

Unlike the analog output by the Pulse Sensor Amped, the MAX3010 operates via I2C protocol with the Feather microcontroller. The reflective PPG measuring principle is the same for both heart rate sensors; only the filtering hardware is slightly different. We want these two heart rate sensors to verify each other's BPM readings and hopefully act as a fail-safe should the sleeve shift position on the forearm during use.

We were not able to record data from actual Rett Syndrome patients at this stage in our device progression, but we were able to take readings from students within the Clemson bioengineering department while they mimic Rett hand stereotypies to the best of their ability. These trials will not provide insight into the biological indicators (i.e. heart rate and galvanic skin response) for Rett patients' abnormal episodes, but they will provide similar motion data to what we expect to receive from a Rett patient. This information can be further analyzed for automatic symptom detection/classification. Therefore, the interesting data we will be looking at for extracting important features from these preliminary trials is the raw EMG, Euler angles,

linear acceleration, and angular velocity. The trials will also offer a better understanding of the capabilities and reliability of the sleeve design.

The setup for each trial entails a brief background of Rett Syndrome, an explanation of the protocol for each trial, and the data acquisition phase. We provide a basic summary of the disease and more specifically describe the hand stereotypies we want the participant to mimic. We then show the participant a few video clips from online sources of Rett patients having an episode of stereotypical periodic hand motions. Tapping, hand wringing, mouthing, and any combination of these three hand stereotypies are the symptoms we have asked our participants to imitate to the best of their ability. Tapping is simply moving the hand up and down periodically. Hand wringing is as if they are washing their hands in a cyclic pattern towards the midline of their body. Mouthing is where they raise their hands towards their face and are periodically tapping their mouth. The protocol consists of three 5:30 minute trials per participant.

Figure 14. 5:30 minute individual trial protocol reminder cues

Within each trial the participant is asked to remain still for the first thirty seconds so the sensors can normalize. After thirty seconds the participant is asked to mimic the tapping motion Rett syndrome patients frequently experience involuntarily for thirty seconds. The participant then moves normally for thirty seconds where they can text, tell a story expressively, any kind of non-periodic motion to express the normal behavior when the Rett syndrome patient is not having an

abnormal episode. The participant is now 1:30 minutes in to the trial; they now reproduce hand wringing behavior for thirty seconds. At 2:00 minutes they again perform normal, non-periodic random hand movements. After thirty seconds of normal hand motion they recreate the mouthing hand stereotypy commonly observed in Rett patients for thirty seconds. At the 3:00 minute mark the participant, again, performs normal hand motions for thirty seconds followed by any combination of hand wringing, tapping, and mouthing until the 4:00 minute cue. The previous minute is repeated from 4:00 minutes until 5:00 minutes where the participant is then asked to remain still at the 5:00 minute mark for thirty seconds until data collection for trial one has concluded. The outlined protocol we have on display for the participants can be seen above in Figure 14. There were fifteen participants for a total of forty-five trials. This data was saved for further analysis.

PRELIMINARY RESULTS AND SENSOR VERIFICATIONS

Figure 15. An example of the linear acceleration (m/s^2) along the y-axis of the BNO055 sensor located on the wrist during one trial

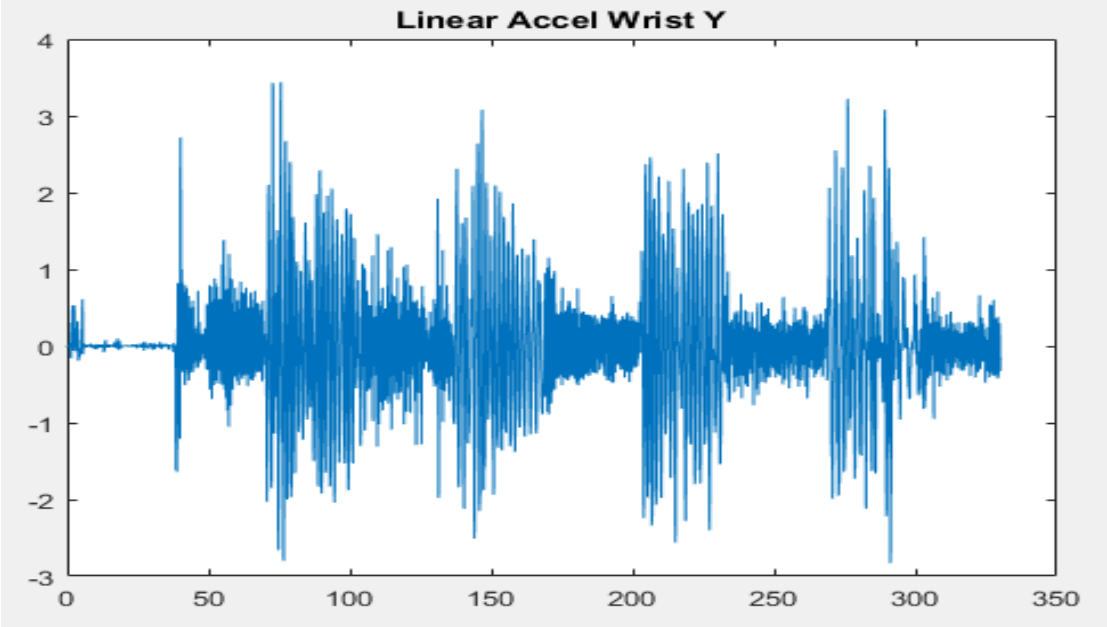

Figure 16. An example of the rotational velocity (m/s) about the y-axis of the BNO055 sensor located on the wrist during one trial

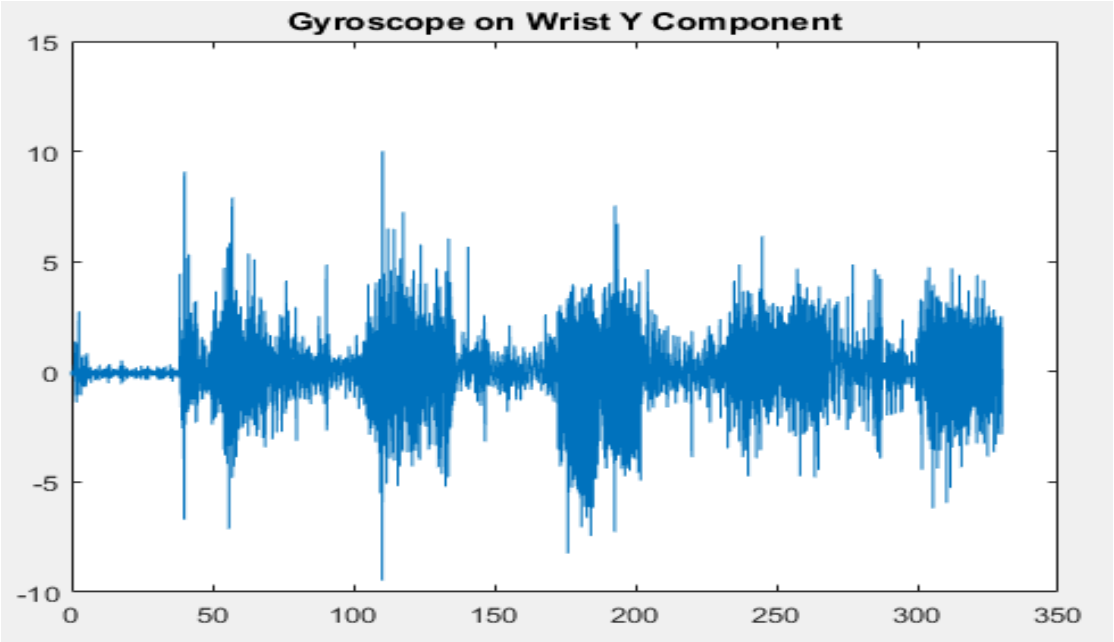

Figure 17. An example of absolute orientation defined as Euler angles (°) along the y-axis of the BNO055 sensor located on the wrist during one trial

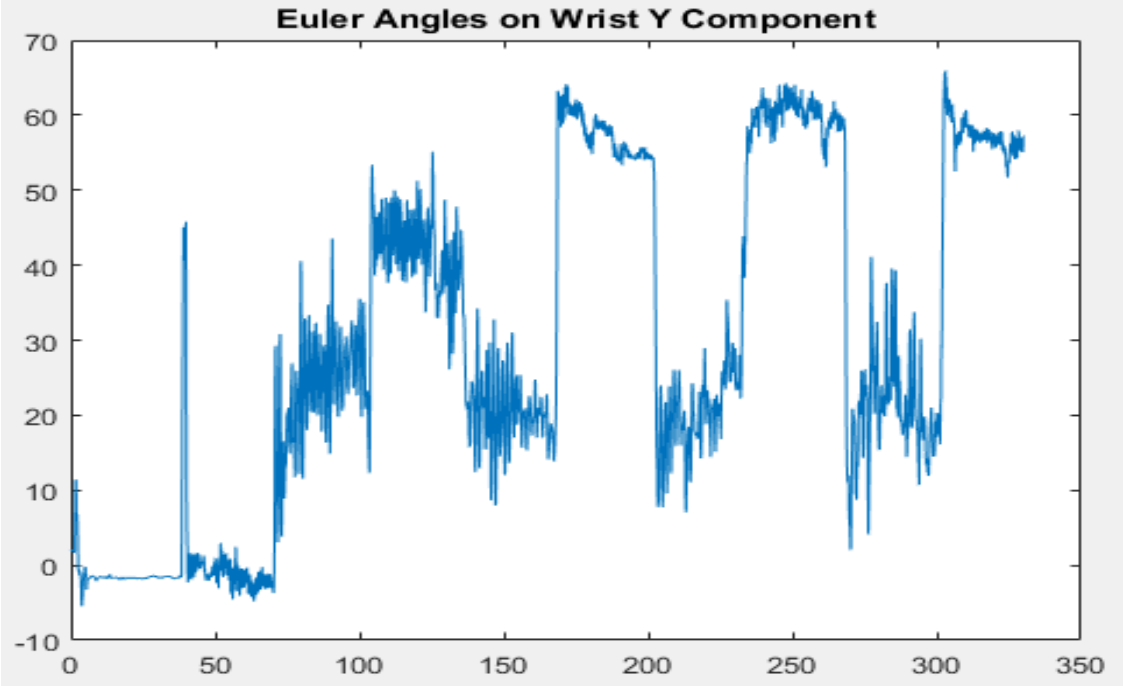

Myoware Muscle Sensor Verification

Statement of Purpose: Electromyography (EMG) is used to detect muscle stimulation through the change in electric potential generated by muscle contraction.[7] EMG data is essential to detecting hand stereotypies in Rett Syndrome: EMG has the ability to determine the magnitude of the muscle contraction to which the electrodes are attached. Our Myoware Muscle Sensor's electrodes are placed in the middle of the extensor digitorum because this muscle is used in varying amounts during phalange, wrist, and elbow extension.[13] The BNO055 sensors on the elbow and wrist are not capable of detecting phalange motion which is important for classifying the type of abnormal episode a Rett patient is experiencing. For instance, phalange extension is periodically different during tapping, hand wringing, and mouthing. In addition, the raw EMG signal will act as a fail-safe for verifying the macro motion data acquired from the two BNO055 sensors.

Methods: In this verification, the sleeve was placed on the participant's arm where the Myoware Muscle Sensor is approximately two to four inches from the elbow and is centered on the posterior of the forearm. The participant was then asked to go through a series of phalange movements that are common to neurodevelopmental disorders and have a higher periodic frequency but a low magnitude in order to test the sensitivity of the sensor. We asked three participants to remain still for thirty seconds and then to perform four movements in thirty second intervals. The list of movements consisted of resting hand tremor (RHT), pill-rolling tremor (PRT), hand writing (HW), and typing (T). This process was performed once while wearing the sleeve with the Myoware Muscle Sensor and once with a Clemson University EMG in combination with the LabTutor software for a total of six trials (three with each EMG).

We used the industry standard wet gel electrodes for the Clemson University EMG (Figure 18) opposed to the novel dry gel electrodes for the Myoware Muscle Sensor. The trials were kept

Figure 18. Clemson University EMG wet gel electrodes on the extensor digitorum

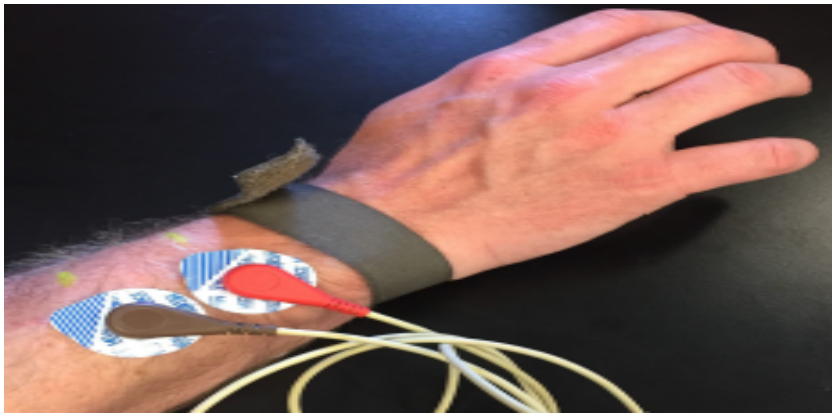

identical with the same approximate lead placement, the same list of motions in the same order, and the same calculation techniques. When one of the four classified motions was being performed we classified it as active state and when the hand remained motionless we classified it as resting state. The relative change in electric potential was determined by calculating the root mean square (RMS) of the electric potential of each of the four active states and then subtracting the RMS of the electric potential associated with the resting state. It has been documented that there is a linear relationship between contraction force and EMG RMS.[14] The average change in electric potential (ACEP) was then calculated by averaging the three trials' relative electric potential changes that were calculated for each of the four motions. The calculated ACEP results were then compared between the sleeve's Myoware Muscle Sensor and the Clemson University approved EMG device (Figure 19).

Results:

Figure 19. Results comparing the average change in electric potential for each hand motion

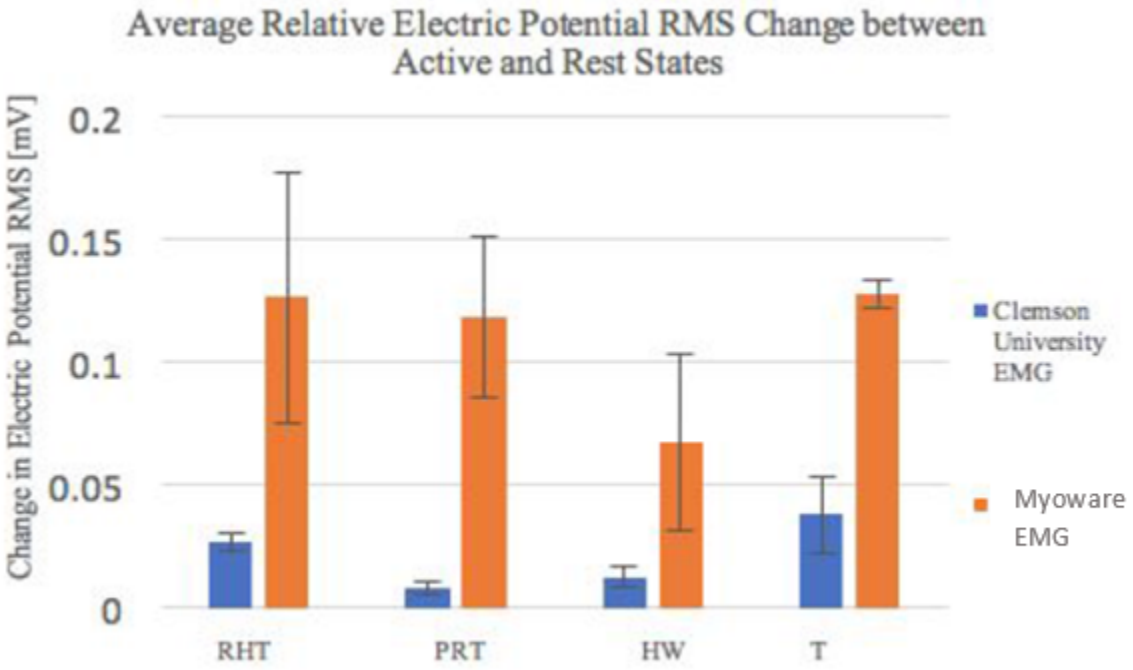

Table 1. Results comparing the average change in electric potential for each hand motion

Subject	Clemson University EMG ACEP ± SD [mV]	Myoware EMG ACEP ± SD [mV]
RHT	0.0268 ± 0.0033	0.1265 ± 0.0508
PRT	0.0080 ± 0.0028	0.1187 ± 0.0326
HW	0.0125 ± 0.0040	0.0674 ± 0.0364
T	0.0379 ± 0.0153	0.1281 ± 0.0059

Conclusions: Both EMG sensors were able to pick up a change in electric potential between active and resting states. The sleeve's Myoware Muscle Sensor recorded a higher electric potential in all four active states but with a slight increase in variability. The elevated electric potential is not concerning because the gain on the Myoware Muscle Sensor can be adjusted if

voltage accuracy becomes important. For our purposes right now, we only need to see a proportional change in electric potential. The Myoware Muscle Sensor passed this verification due to its ability to detect a noticeable change in electric potential which can be later used to determine if a Rett Syndrome hand stereotypy is taking place.

BNO055 Motion Sensor Verification

Statement of Purpose: The sleeve must be able to record samples at a sufficiently high frequency so that important motion data will not be missed. The highest periodic motion frequency we expect to encounter with a Rett Syndrome patient will be in the form of a low magnitude, rapid jitter or a tremor. Table 2 details three common tremors and their known frequencies.

Table 2. Known characteristics of involuntary movement disorders

Condition	Tremor *f* range	Resting, postural, action?
Parkinson's Disease	Low: 4-6 Hz	Resting
Essential Tremor	Medium: 5-8 Hz	Postural / Action
Orthostatic Tremor	High: 14-18 Hz	Action

Methods: The BNO055 was tested at 4, 7 and 18 Hz, which represented the low, medium, and high-end frequencies of common movement disorders. We secured a platform to an old speaker which can be seen in Figure 20; the speaker acts as our medium for oscillation. The input voltage given to the speaker was set to Vin = 5V and the function generator was set to recreate a sine wave at the frequency of interest. The BNO055 was then secured to the platform and turned on. Next, the exact procedure for each frequency is detailed in Table 3, three trials per frequency. For example, we recorded four minutes of motion data for 7 Hz three separate times.

Figure 20. BNO055 platform attached to oscillating speaker

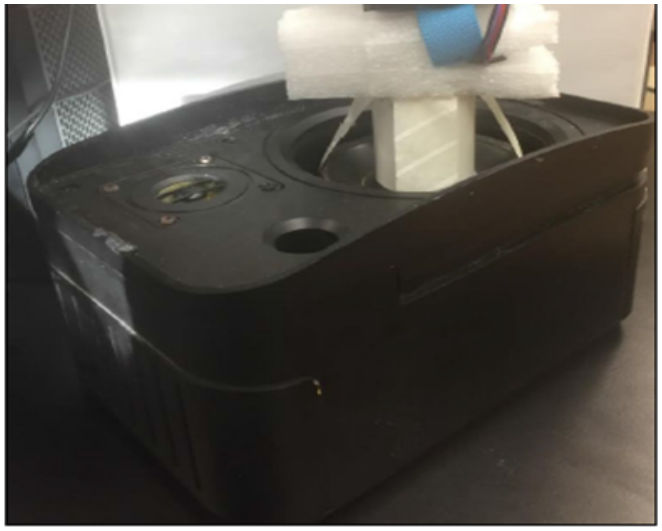

Table 3. Protocol for data acquisition at each frequency

Time (minutes)	4 Hz	7 Hz	18 Hz
0 - 0.5	Rest	Rest	Rest
0.5 - 2.5	Motion	Motion	Motion
2.5 – 3	Rest	Rest	Rest
3 - 5	Motion	Motion	Motion

The motion data was converted into frequency domain (Figure 21), so we could compare the recorded frequency to the known input frequency (Figure 22). The average correlation coefficient was recorded for each frequency to determine precision.

Results:

Figure 21. BNO055 motion data converted to frequency (Hz) domain

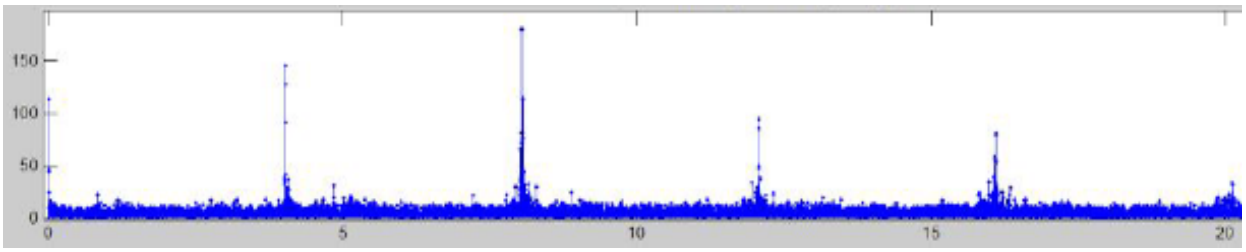

Figure 22. Function generator input frequencies compared to motion data frequencies

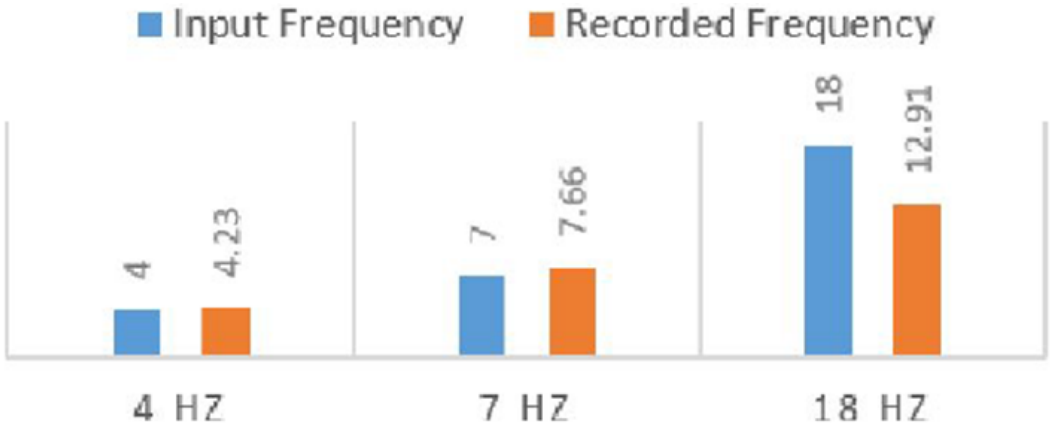

Table 4. Correlation coefficient between trials recorded at the same frequency

	4 Hz	7Hz	18Hz
Correlation Coefficient	0.774	0.737	0.125

Conclusions: The BNO055 verification test was a success. It can be clearly seen in Figure 21 that the predominant frequencies recorded were at 4 Hz, 7 Hz, 13 Hz, and 18 Hz. In Figure 22 and Table 4 it can be easily seen that the BNO055 is able to accurately and precisely record periodic motion data at frequencies of 4 Hz and 7 Hz. The reason there are frequencies being recorded around 13 Hz is due to the platform design not moving as one with the speaker at frequencies as high as 18Hz; the poor correlation coefficient and inaccuracy of the trials at 18 Hz is not due to the sampling rate of the BNO055 being set below the Nyquist frequency. We would also like to note that it is unlikely Rett Syndrome patients will experience hand stereotypies with frequencies anywhere near 18 Hz unless they are diagnosed with orthostatic tremors in addition to Rett Syndrome. For these reasons we pass the BNO055 as a sufficient sensor for tracking periodic motion.

Galvanic Skin Response Sensor Verification

Statement of Purpose: We are looking to investigate whether or not biological signals can serve as precursors to tremors and other symptoms of neurological movement disorders, specifically dyskinesia, dystonia, and gait impairment related to Rett Syndrome.[16] In our Rett Syndrome sleeve, detection of changes in heart rate and/or galvanic skin response will be analyzed to determine symptom presence and severity. One biological signal of interest is Galvanic Skin Response (GSR); GSR can change in response to stress, discomfort, or in reaction to unexpected circumstances, such as a tremor or other abnormal periodic episodes. It is, therefore, critical to verify that the GSR electrode placement on our sleeve permits the sensor to function accurately and precisely during patient free living in everyday life. To ensure this is the case, GSR electrodes will be tested on the recommended location, the fingers, and our sleeve's electrode location (Figure 1).

Methods: This verification study used five healthy subjects for two trials each. Each participant is first told how the test will operate, then the Grove GSR electrodes are placed on the subject's fingers (Figure 23). Next, the participant is instructed to sit on an Epic A17u Upright Exercise

Figure 23. Grove's recommended electrode position for measuring galvanic skin response

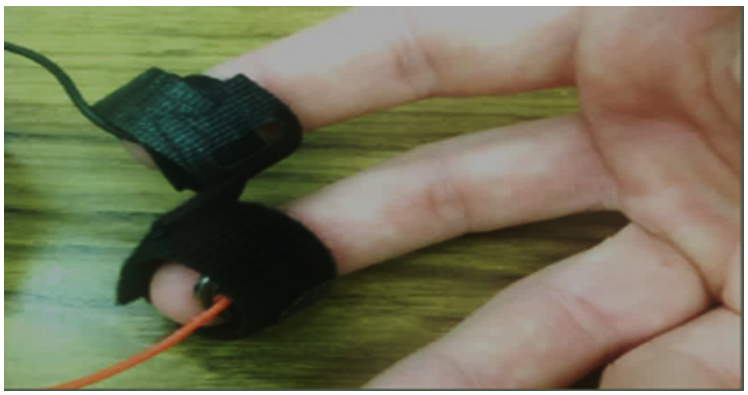

Bike, and the device begins recording for a period of six minutes. The intervals of resting and pedaling are outlined in Table 5. Ten minutes after the first trial, when the electrodes are on the fingers is completed the participant is then asked to wear the sleeve and perform the same resting/pedaling tasks. The data from trial 1 is compared to trial 2 by finding a correlation

Table 5. Individual trial protocol for resting/pedaling while measuring the galvanic skin response

Time (minutes)	0-1	1-2	2-3	3-4	4-6
Rest Pedal (50-60 RPMs)	Rest	Pedal	Rest	Pedal	Rest

coefficient (Table 6).[15] This comparison ultimately aims to highlight the similarities between the clinically accepted value produced by the placement of the electrodes on the fingers versus our sleeve electrode placement.

Results:

Figure 24. One trial with electrodes on fingers where normalized resistance is plotted over sample number

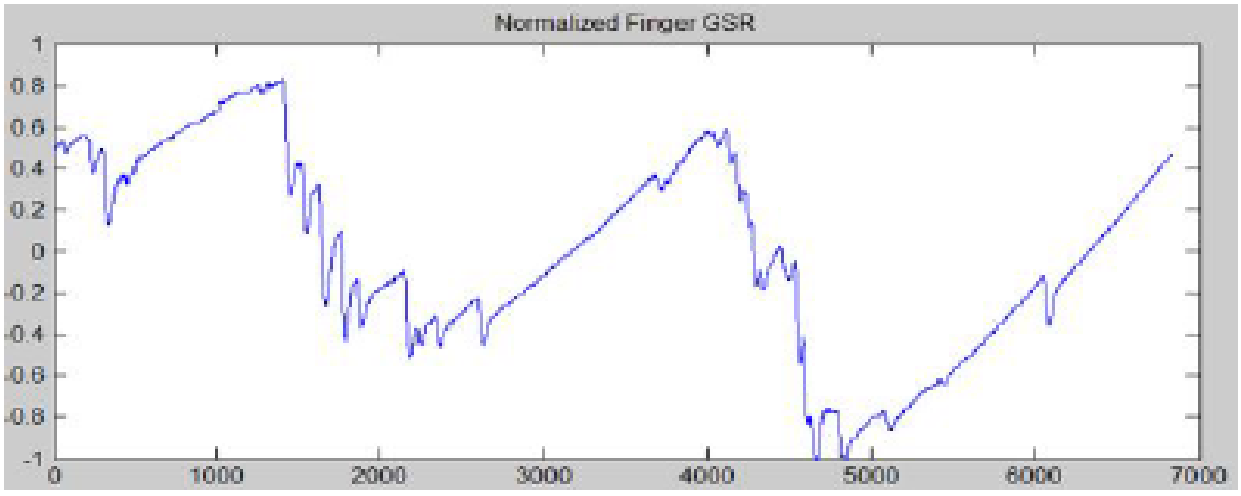

Figure 25. Subsequent trial with electrodes at forearm location where normalized resistance is plotted over sample number

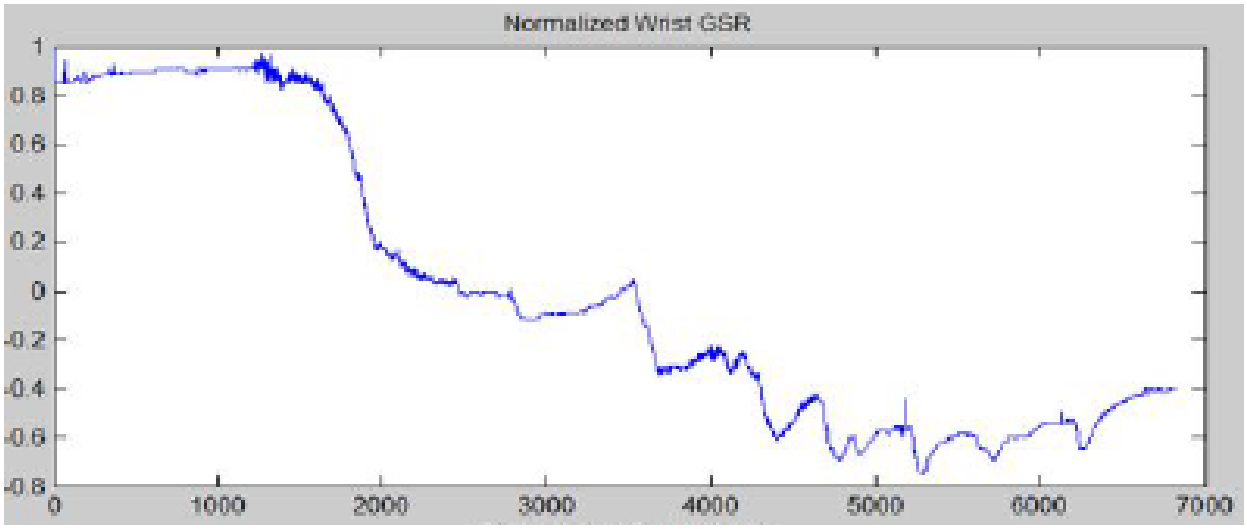

Table 6. Five participants with a corresponding correlation coefficient comparing efficacy of two trials' electrode position

Subject	1	2	3	4	5
Correlation Coefficient	0.702	0.659	0.625	0.501	0.711

Conclusions: Both GSR electrode placements, on the fingers and forearm, do successfully measure resistance of the skin. For example, both sets of data exemplify a decrease in resistance once the subject began pedaling. Unfortunately, the resistance recorded by the sensors on the fingers tended to rapidly normalize during resting periods while the resistance of the sleeve's electrodes on the forearm failed to normalize. The average correlation coefficient was 0.640 which is a positive correlation coefficient, but not quite our target of at least 0.70. We used correlation as a method of assessing the association between two continuous variables, one being GSR data from the forearm and the other from the fingers.[15] Improvements in testing design

could include looking for shifts in general trends of resistance rather than a direct correlation. A probable explanation for the sleeve's electrode placement not allowing the resistance reading to normalize could be due to the sleeve preventing the skin in contact from drying at the natural rate. The average correlation coefficient is below 0.7, so the Galvanic Skin Response Sensor failed this verification due to its inability to reliably measure a change in skin resistance when electrodes are placed anteriorly at the proximal and distal ends of the forearm.

Pulse Sensor and MAX3010 Verification

Statement of Purpose: It is known that non-motor biological signals can serve as precursors to tremors and other symptoms of neurological movement disorders, such as dyskinesia and gait impairment.[16] Another biological signal of interest is heart rate, elevated heart rate is indicative of the subconscious anxiety that a patient experiences prior to a symptomatic episode.[17] We also would like to record heart rate during abnormal episodic behavior in Rett patients to document any interesting fluctuations from the patient's normal heart rate. It is therefore critical to verify that the Rett Syndrome sleeve's heart rate monitoring system is functioning accurately and precisely during patient free living of everyday life.

Methods: We used five healthy subjects with no known heart conditions for four 1-minute trials (20 trials total). Subjects placed the Clemson finger heart rate monitor onto the distal phalanx of their right index finger and secured the monitor in place using a Velcro strap (Figure 26).

Figure 26. Clemson University heart rate monitor secured to the right index finger

The finger heart rate monitor was hooked into the lab monitor and a steady pulse wave was obtained in LabChart. Simultaneously, the sleeve was put on and adjusted so the Pulse Sensor was snuggly on the posterior wrist and the MAX3010 was secured over the wrist's radial artery. A timer was set for t = 1 minute, and all three devices collected the raw heart rate signal. After one minute, data collection was stopped and analyzed. The data collected from the Clemson University heart rate finger monitor was visualized and interpreted via the LabChart program where beats per minute (BPM) were easily calculated via peak-to-peak method (Figure 27).

Figure 27. Clemson University heart rate finger monitor's raw PPG waveform displayed in LabChart with peak-to-peak demarcation for BPM calculations

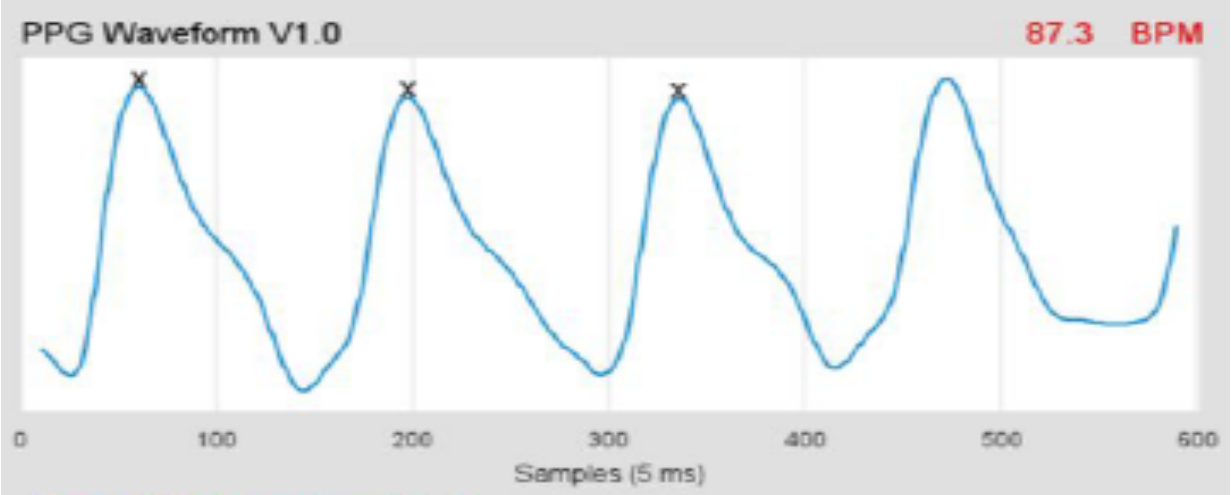

The data collected from the Pulse Sensor and the MAX3010 each have a program written to determine the BPM; these BPM readings are then averaged and are now ready for comparison.

Results:

Table 7. Clemson University heart rate finger monitor's BPM compared to the averaged BPM of the MAX3010 and Pulse Sensor

Subject	Finger Monitor Heart Rate Mean ± SD [bpm]	Pulse Sensor and MAX3010 Averaged Heart Rate Mean ± SD [bpm]
1	87.75 ± 2.22	88.5 ± 3.50
2	70 ± 2.16	71.75 ± 1.71
3	63.0 ± 0.82	64 ± 0.82
4	76.5 ± 1.73	77.25 ± 2.63
5	82.5 ± 2.38	80 ± 1.83

Figure 28. Graphical representation of the comparison between heart rate monitoring devices

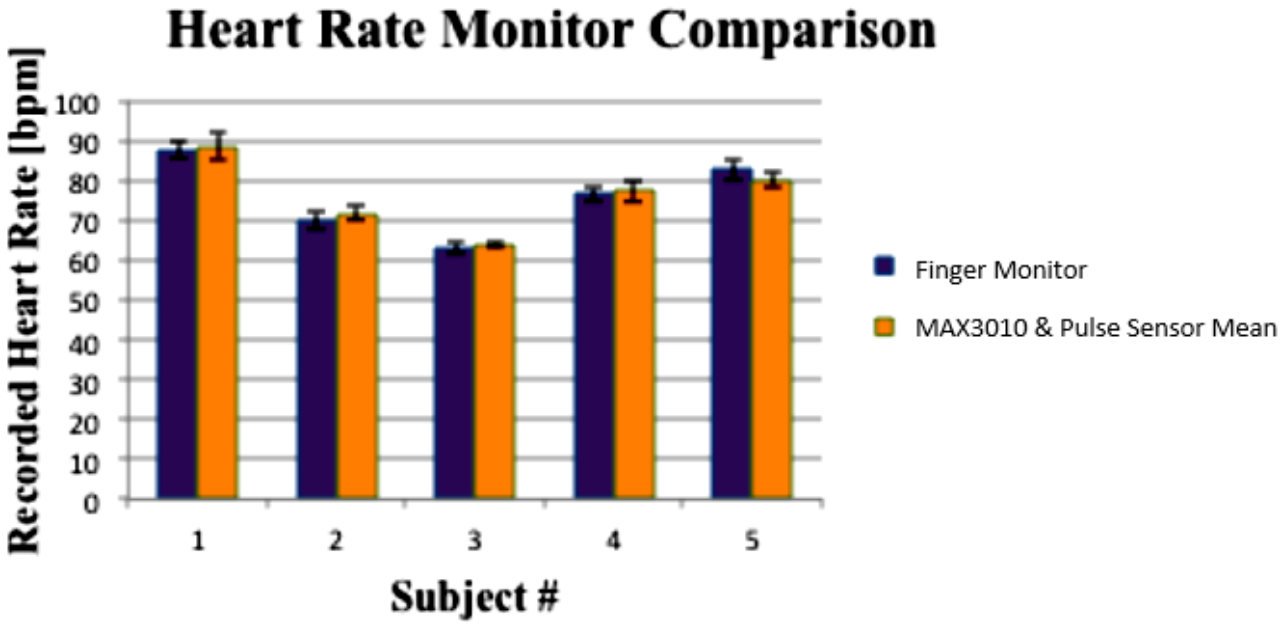

Conclusions: As seen in Figure 28 and Table 7, the mean BPM of the MAX3010 and Pulse Sensor when placed on the wrist are on average off by less than 1.35 bpm from the industry standard finger pulse monitor. The sleeve's heart rate analysis and sensor location pass this

verification test due to their ability to reliably measure beats per minute as long as the sleeve is secured in the desired position.

CONCLUSIONS

The verification tests were necessary to prove the sensors we have chosen not only operated to the manufacturers' specifications but that the sensors were capable of operating reliably and accurately within the patient environment. The EMG and BNO055 sensors proved to accurately record periodic motion data at frequencies closely associated to Rett syndrome and similar diseases. Having a BNO055 sensor at the elbow and wrist allows us to interpret the orientation of the arm during the abnormal episodes of Rett Syndrome. If the patient is simply tapping her hand then little to no motion will be present at the elbow but periodic motion at the wrist will be present. If the patient is wringing her hands then there is a certain degree of twisting of the forearm involved. This means the Euler Angles, linear acceleration, and rotational velocity data will have different distributions and amplitudes at the wrist and elbow. The amplitude of the EMG will also vary depending on the type of hand stereotypy the patient is experiencing. This is important to note moving forward with this project because the more data that indicates the type of hand stereotypy a patient is experiencing the more confident we can be in an automatic episode classification algorithm.

It has yet to be determined if the heart rate or galvanic skin response of the patient will provide any indication that the patient is experiencing an abnormal episode. This can only be determined by recording data on patients who have Rett syndrome. We wanted to still go ahead and verify the two heart rate sensors and galvanic skin response sensor were able to record accurately. The heart rate sensors are absolutely able to record beats per minute when placed on the wrist opposed to on a finger which is very promising; however, a key issue that must be

addressed in any wearable biometric device is the inevitability that the sensors may not remain in the desired location resulting in a discontinuous data stream. For this reason, we placed two heart rate sensors in two different locations in hope that at least one of them will be able to pick up the heart rate of the patient at any given time. Moving forward with the project, it needs to first be determined if heart rate is a useful metric for determining the duration, severity and type of hand stereotypy the Rett patient is experiencing. If it is determined heart rate is a useful metric then a method for reliably measuring heart rate utilizing these sensors must be employed.

The galvanic skin response sensor accurately recorded data when the electrodes were placed on the fingers but failed to accurately record data when placed at the proximal and distal ends of the forearm. This failure is most likely due to the sleeve itself not allowing the skin beneath the sleeve to be exposed to the air directly. The galvanic skin response sensor relies on the change in resistance between the two electrodes and if the sleeve is not allowing perspiration to evaporate properly then the resistance measurement will be inaccurate. Moving forward it must be determined if galvanic skin response is a useful metric for determining duration, severity, and type of hand stereotypy Rett syndrome patients are experiencing. If it is determined galvanic skin response is a useful metric then the proper placement of the electrodes for accurate and reliable data acquisition must be addressed.

The Rett sleeve provides a novel way of measuring patient symptoms and offers unprecedented insight about the disease itself. Having a noninvasive continuous monitoring system allows the clinician to quantify the duration, severity, and type of symptoms the patient is experiencing. This is important because the clinicians' only form of information currently comes from what they observe in the clinic and what the parents of the patient tell them. Data collected in the clinic often can be skewed as a result of the patient being in an intimidating, unfamiliar

setting. Unbiased, at home data is important for understanding the mechanics of the disease and the lifestyle of the patient. This sleeve does not only have the potential for helping clinicians better understand Rett syndrome but also many neurodevelopmental disorders such as Parkinson's disease, essential tremor, autism spectrum disorder, and many others. Biometrics is a quickly growing industry affecting everyday life in the form of measuring vitals and tracking fitness; applying the same sensor based methodology to patients is the future of improving quality of care.

REFERENCES

[1] O'Leary, H.M., Marschiki, P.B., Khwaja, O.S., Ho, E., Barnes, K.V., Clarkson, T.W., Bruck, N.M., & Kaufmann, W.E. (2015). Detecting autonomic response 1751-8431. doi: to pain in Rett syndrome. Developmental Neurorehabilitation, 10.3109/17518423.2015.1087437

[2] Guy, J., Hendrich, B., Holmes, M., Martin, J.E., & Bird, A. (2001). A mouse Mecp2-null mutation causes neurological symptoms that mimic Rett syndrome. Nature Genetics, 27, 322-326. doi:10.1038/85899

[3] "About Rett Syndrome." *RettSyndrome.org*, www.rettsyndrome.org/about-rett-syndrome.

[4] Industries, Adafruit. "Adafruit Industries." *Adafruit Industries Blog RSS*, www.adafruit.com/.

[5] "I2C Info – I2C Bus, Interface and Protocol." *I2C Info – I2C Bus, Interface and Protocol*, i2c.info/.

[6] "MyoWare Muscle Sensor." *SEN-13723 - SparkFun Electronics*, www.sparkfun.com/products/13723.

[7] "MeSH Browser." *U.S. National Library of Medicine*, National Institutes of Health, meshb.nlm.nih.gov/record/ui?name.

[8] "Electrode Specifications." *Drypad Sensors (for Skin)*, www.cognionics.com/index.php/products/sensors/drypad.

[9] "Bosch Sensortech." *BNO55*, www.bosch-sensortec.com/bst/products/all_products/bno055.

[10] Team, Seeedstudio. "Grove - GSR Sensor." *Seeed Wiki*, wiki.seeed.cc/Grove-GSR_Sensor/.

[11] "Pulse Sensor." *World Famous Electronics Llc.*, pulsesensor.com/.

[12] “MAX3010” *Maxim*, www.maximintegrated.com/en/products/interface/level-translators/MAX3010.html.

[13] Moore, Keith; Anne Agur (2007). *Essential Clinical Anatomy, Third Edition*. Lippincott Williams & Wilkins. ISBN 0-7817-6274-X.

[14] Fukuda, Thiago. *Root Mean Square Value of the Electromyogarphic Signal*. The Journal of Applied Research. 2010; Vol. 10, No. 1.

[15] Mukaka, MM. “A Guide to Appropriate Use of Correlation Coefficient in Medical Research.” Malawi Medical Journal: The Journal of Medical Association of Malawi 24.3 (2012): 69–71.

[16] Espay AJ, et al. (2016) *Technology in Parkinson’s Disease: Challenges and Opportunities*. Mov Disord, 31, 1272–1282.

[17] Devos D, Kroumova M, Bordet R, et al. *Heart rate variability and Parkinson’s disease severity*. J Neural Transm. 2003; 110:997–1011.

CHAPTER TWO: ANALYZING ARTERIOVENOUS FISTULA CANNULATION SKILL

INTRODUCTION

Kidneys are organs in the body that are integral in the blood purification process. Loss of kidney function can potentially lead to the diagnosis of Chronic Kidney Disease (CKD). The final stage of CKD is known as End Stage Renal Disease (ESRD).[4] Treatment options for ESRD are extremely limited. The only methods available to sustain life for patients with ESRD are to (1) receive a kidney transplant which could take years to find a match, or (2) to undergo dialysis treatments. In the United States alone, there are 100,000 people on the transplant list but fewer than 20,000 donors are able to be considered.[1] This leads to the increased reliance on dialysis, (both hemodialysis and peritoneal dialysis) for ESRD patient treatment.

There are two kinds of dialysis: hemodialysis and peritoneal dialysis. Hemodialysis is the far more common type of dialysis in the United States—about 90% of all dialysis patients.[1] Hemodialysis requires the patient to undergo dialysis three to four times a week, at approximately four hours per session. Hemodialysis is a tedious procedure to perform correctly, requiring the technicians to have a high degree of skill. In order to run blood through an external dialyzer, a patient must first have a vascular access created by a surgeon by joining an artery to a vein naturally (AV fistula) or synthetically (AV graft). The AV fistula or graft will then be the target area to cannulate.[2] In the dialysis clinic, technicians are required to locate the AV fistula, find a proper cannulation site, and cannulate the fistula in order to externally purify the blood using a machine known as a dialyzer (Figure 29).[3,5] These steps require meticulous care and skilled expertise in order to conduct the procedure proficiently. Unfortunately, there are currently

very limited resources or systems that are proven to be effective in training technicians to properly palpate for the fistula or accurately cannulate the fistula with a needle. Most nurses and technicians feel somewhat comfortable cannulating mature fistulas if they are superficial, large, and straight enough to allow for safe insertion of two needles (one for arterial side and another for venous).[5] In order to locate the ideal site for cannulation, nurses are taught to use the "thrill" and "bruit" of the fistula. The thrill refers to the constant vibration that is distinguishable from the pulses that can also be felt. The bruit refers to the constant whooshing sound that is a result of the blood flowing through the fistula.[2] These are generally the only cues used by nurses and

Figure 29. The circuit for typical hemodialysis

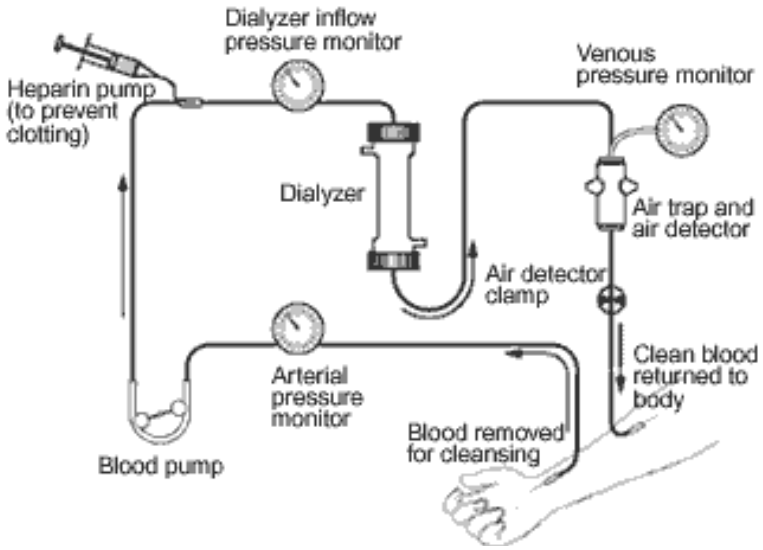

technicians prior to cannulation. Cannulation-related medical errors are a significant concern in the medical community due to the high frequency or failed cannulation cases and the cascade effect of related morbidities. Recent studies reveal that only 35% of hemodialysis patients remain alive after five years of treatment.[1] Patients are less likely to consistently meet all of their dialysis appointments and needs if cannulation procedures are an uncomfortable or even painful experience due to improper cannulation technique. Therefore, there is a growing need for an

improved training protocol that adequately provides the necessary skills to inexperienced technicians to safely and effectively cannulate ESRD patients.

RESEARCH DESIGN AND METHODS

The experimental study heavily relies on three primary physical components: the cannulation simulator, a camera, and the Leap Motion® sensor. A stand was constructed to place the Leap Motion® sensor and camera 43 cm and 81 cm respectively above the simulator.

Simulator

The cannulation simulator consists of a plastic outer shell, of 58.50 cm diameter, and six even “pie piece” sections of foam that span the six distinct regions that will be felt during palpation. Each region houses a fistula module that may be vibrating for the duration of each trial in the experiment (Figure 30).

Figure 30. Cannulation simulator setup with Leap Motion® sensor and camera

Our six model fistulas are dimensioned at 3 x 3 x 14.5 cm, with the target region raised with an area of 1.75 x 14.5 cm (Figure 31). The target region is meant to represent a mature fistula. During an experimental task, a fistula is placed randomly in each of the six regions such that it is not readily obvious for the participant to determine its location. Vibration motors, connected to the underside of both end points of each fistula, provide vibratory stimuli approximating "thrill". The vibratory stimulus is similar to the thrill that can be felt on a mature AV fistula. Of the six fistulas, only one pair of vibration motors will be buzzing at a time during a single trial; therefore, the vibrating fistula's target region is the desired cannulation location. Custom written software allows us to cycle through which one of the six fistulas is to vibrate for the current trial.

Figure 31. One of six fistula modules

The final element of the simulator is the synthetic skin that is placed on the top of the simulator (Figure 32). The synthetic skin was created using cured silicone rubber material from Ecoflex series (Smooth-On Inc.). Ecoflex has a set cure time but can be shaped into whatever mold it is poured in before it cures. The silicone and rubber components give the skin an elastic, loosely dense feel.

The synthetic skin hides the position of the six fistulas, but when palpated on it is still discernable whether or not there is a fistula or only foam underneath.

Figure 32. The simulator without and with the synthetic skin layer

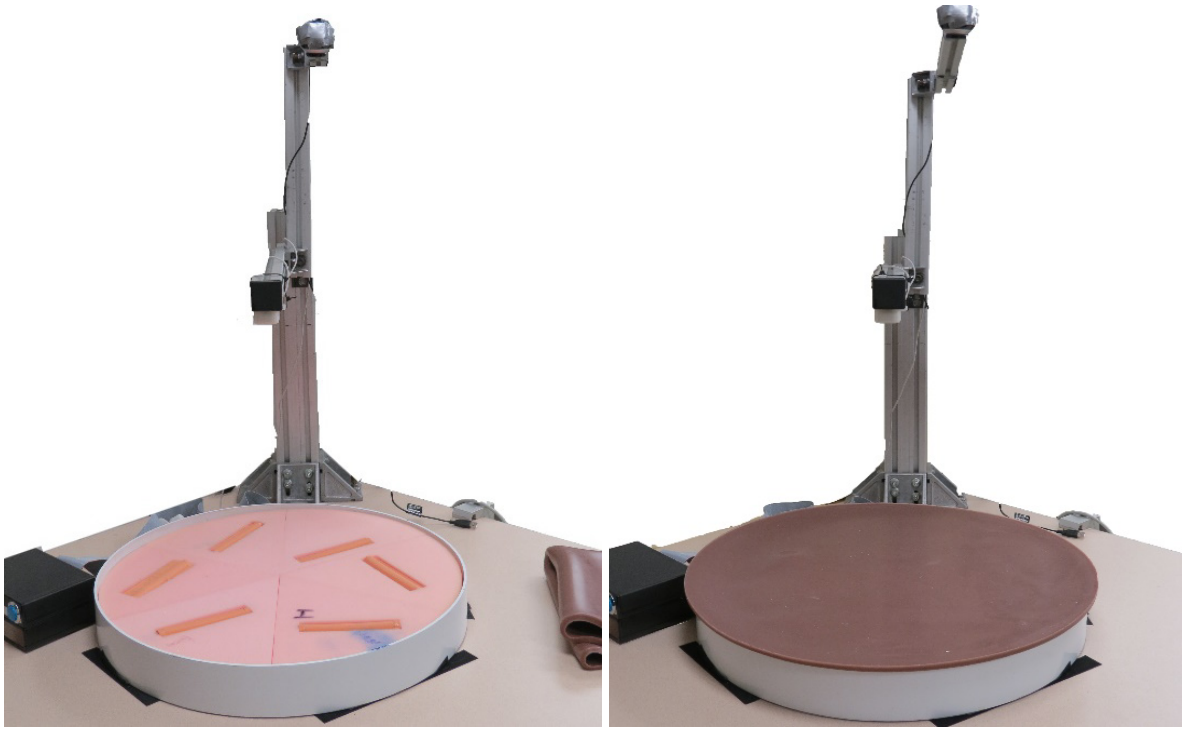

Camera

A camera was included in our design to allow for visualization of hand movement during palpation. Since we didn't plan on using the camera for post-image processing, we did not need a high end, rapid frame rate camera. For instance, we need to be able to watch the video of the trial and record what times the participant started, found the cannulation location, and stopped palpating. Following this, we would look at the recorded data from the Leap Motion® sensor at those recorded time points of interest. We chose to use an HP Pro Webcam, rated to record at 30 frames per second for smooth and natural body motion at a 640 x 480 video resolution (Figure 33).[6] The HP Pro webcam easily integrates to the computer via USB 2.0 connection and can be

used as the computer's default camera once the driver is installed. We utilized the Open Source Computer Vision Library (OpenCV) to integrate the webcam into our program.

Figure 33. HP Pro webcam

One limitation of this webcam is that the field of view is not wide enough to be placed at the same height as the Leap Motion®; consequently, the camera had to be placed 81 cm above the plane of the simulator in order to capture the entire palpation area.

Leap Motion® Sensor

A crucial piece of information that must be observed is the palpation behavior of the subject when searching for the source of the fistula thrill. Finding the thrill source is one of the most challenging aspects of the cannulation procedure. Although this seems to be a relatively standard procedure in nursing, tracking hand movement may lead to more methodical teaching practices that can improve cannulation training. In order to track the hand movement of participants, many options for a motion capture device were considered. It was essential to find a camera that was able to accurately and precisely record instantaneous finger positions at a sufficiently high sampling rate for at least a single hand.

The Leap Motion® controller is the ideal selection, as its motion capture system was able to reliably track hand movements. The accompanying application program interface (API) is extremely versatile and permits a wide variety of metrics to be extracted from the user's hand. The Leap Motion® controller is most commonly used as novel interface on Virtual Reality applications to track the movement of hands. The software developer kit for the Leap Motion® controller allows the user to interact with a virtual object by rendering the user's hand(s) into the virtual environment (Figure 34).[7] Originally, the Leap Motion® controller was designed to be placed on a flat surface with its sensors facing upward and reading the movement of hand motion

Figure 34. The Leap Motion® controller allowing interaction with the virtual world

from underneath the user's hands. Due to the increased use of the Leap Motion® controller in virtual reality applications, the Leap Motion® controller has improved adaptability in being able to reliably track hand movement from above the user's hands.[7] In this study, we will be taking advantage of the Leap Motion® controller's ability to read precise and accurate hand movements in order to observe the palpation methods used by participants attempting a cannulation task.

The Leap Motion® controller uses infrared (IR) imaging to recognize and track hands, fingers, and finger-like tools. It may be postulated that the Leap Motion® controller employs

Figure 35. Leap Motion® controller exploded for sensor and camera visualization

a stereo vision technique (as there are two cameras used in combination) in order to determine the precise depth of the particular object in its field of view. The heart of the device consists of two cameras and three infrared LEDs which allows the Leap Motion® to track infrared light at a wavelength of 850 nm (Figure 35).[7] The middle IR emitter that is placed at the center of the front

Figure 36. Interaction volume with respect to Leap Motion® origin is 2 ft above the controller, by 2 ft wide on each side (150° angle), by 2 ft deep on each side (120° angle)

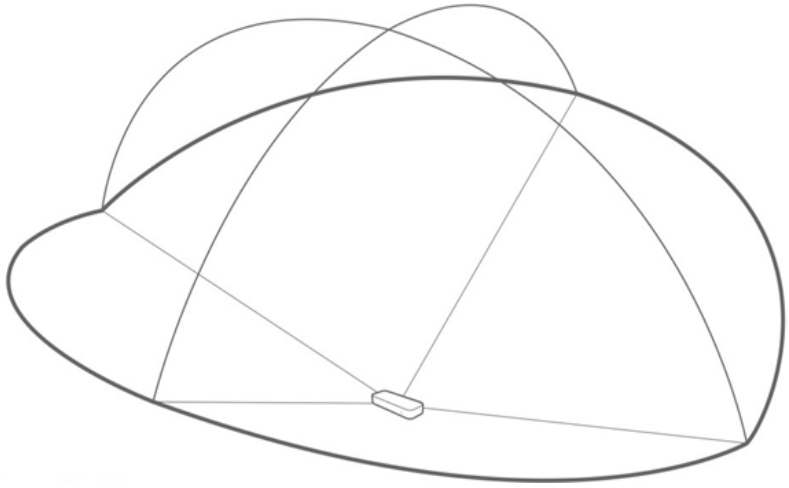

side of the Leap Motion® controller is referred to as the origin. The Leap Motion® controller is able to determine a host of features (which can be found on the API library), and this is due to its ability to determine the position of the object relative to the origin (designated as (0,0,0)). The

field of view from the origin is an inverted pyramid with a range from 25 to 600 millimeters (Figure 36).[7] The data takes the form of a grayscale stereo image of the near-infrared light spectrum, separated into the left and right cameras (Figure 37). Images are then analyzed to

Figure 37. Stereoscopic gray scale image taken by Leap Motion®

reconstruct a 3D representation of what the device sees. The tracking layer matches the data to extract tracking information such as fingers and tools.[7]

These characteristics of the Leap Motion® controller make it a very suitable choice for capturing and observing precise hand and finger movement within a confined space. In this study we will be using the Leap Motion® controller to record the positional data of the five fingers during palpation as well as the tip velocities for each finger. The next logical step was to verify the accuracy and precision of the five finger's position data to ensure the Leap Motion® controller can provide us with sufficient resolution for tracking palpation.

Leap Motion® Static Position Error Verification

Procedure: We placed our index finger at the furthest most point of both ends of the six fistulas and recorded the twelve coordinates (x,y,z) using the Leap Motion®. We then measured these same points from the origin of the simulator using a protractor and ruler (= real locations).

A t-test was then used to compare the Leap Coordinate's distance from the origin to the measured distance from the origin. Another t-test was then performed to compare the Leap Coordinate's tangent angle to the measured protractor angle with respect to the negative x axis. Figure 39 demonstrates the orientation of the Leap's axes with respect the simulator. An example procedure for measuring the distance from the origin to the fistula endpoints as well as measuring the angle from the negative x axis to the same two endpoints on the fistula can be seen in Figure 38. Results can be seen below in Table 8.

Figure 38. Leap Motion® static position accuracy verification example

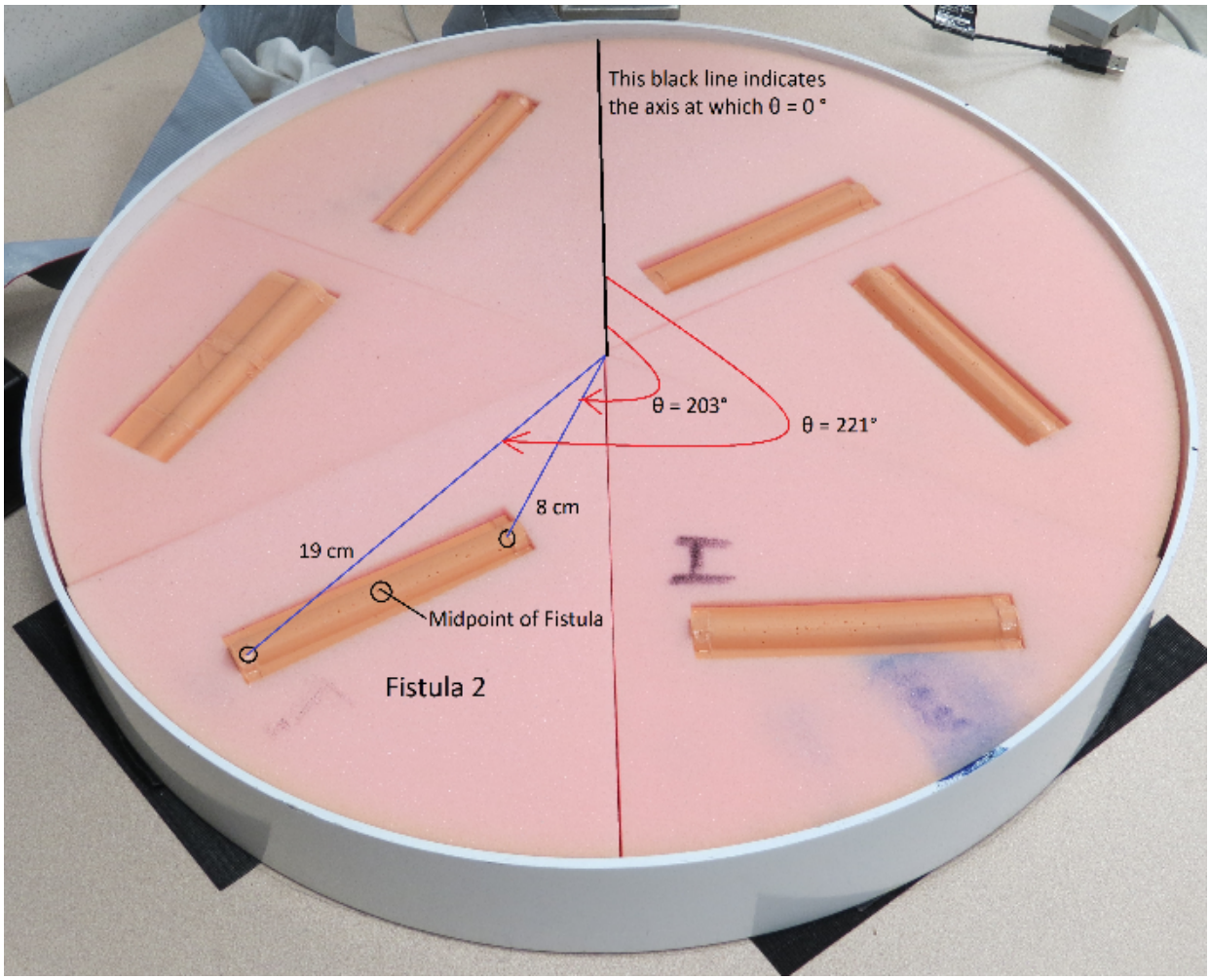

Table 8. Leap static position accuracy verification results

Fistula ID	x	y	x^2*y^2	Distance to Origin measured by Leap (mm)	Distance to Origin measured by Ruler (mm)	Difference (mm)	Mean Difference (mm)	Pvalue
F1	179.182	32.941	33191.345	182.185	187.000	4.815	9.102	0.006
	194.204	141.223	57659.018	240.123	243.000	2.877		
F2	112.186	-57.141	15850.827	125.900	133.000	7.100		
	167.816	-153.948	51862.430	227.733	243.000	15.267		
F3	-52.001	-155.863	26997.389	164.309	173.000	8.691		
	47.023	-223.285	52067.154	228.182	236.000	7.818		
F4	-108.452	-107.816	23386.124	152.925	163.000	10.075		
	-211.367	-29.188	45527.959	213.373	230.000	16.627		
F5	-51.658	32.396	3718.035	60.976	71.000	10.024		
	-99.955	146.410	31426.978	177.277	189.000	11.723		
F6	80.788	219.849	54860.556	234.223	222.000	12.223		
	-59.187	148.634	25595.080	159.985	158.000	1.985		

Fistula ID	Angle from -X axis measured by Leap (deg)	Angle from -X axis measured by Protractor (deg)	Difference (deg)	Mean Difference (deg)	pvalue
F1	169.583	166.000	3.583	3.064	0.003
	143.976	140.000	3.976		
F2	206.992	203.000	3.992		
	222.532	221.000	1.532		
F3	288.451	285.000	3.451		
	258.108	258.000	0.108		
F4	315.169	316.000	0.831		
	352.138	347.000	5.138		
F5	32.092	29.000	3.092		
	55.678	50.000	5.678		
F6	69.823	72.500	2.677		
	111.713	109.000	2.713		

Figure 39. The Leap axes labeled with respect to the controller's orientation in the experiment

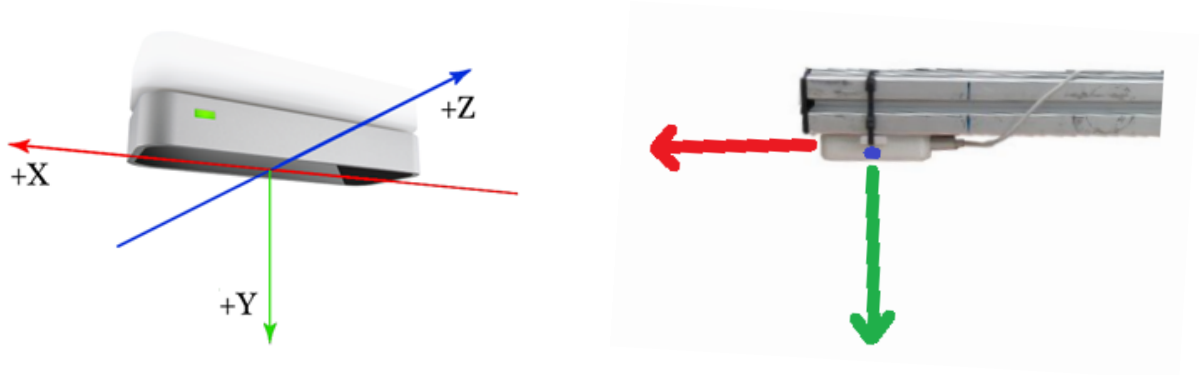

After repeating this procedure three times to ensure precision, results indicate that the Leap coordinates accurately indicate the physical location of the cannulation simulator with a mean difference of 0.9 cm and 3° with p-values less than 0.05 consistently.

Protocol

For each trial, the participant was asked to wear a white glove and to keep his or her hand above the simulator for five seconds to allow for the Leap Motion® sensor to calibrate. The white glove causes a greater grayscale contrast between the simulator's skin tone and the palpating hand which increases the reliability of the Leap. After the calibration phase was complete, the participant was permitted to physically place their hand on top of the simulator, at which point the experiment's timer was started. The participant then would palpate, feeling for differences in structure beneath the skin as well as differences in vibratory stimulus in order to determine an appropriate cannulation location along the indicated fistula. When the participant felt he or she had reached an acceptable cannulation entry point, they placed their index finger on the location and verbally notified the experimenter. After finding one location, the participant was asked to find two other acceptable points of entry along the same fistula approximately one inch apart if possible. Once the third point was identified, the trial was concluded. Each participant underwent three separate trials; the first and the third trials were for the fistula on which we will be performing palpation analysis. The second trial had a random, non-pertinent fistula vibrate for the participant to find via palpation. Once the three trials were concluded, the experiment was complete.

Data Acquisition

During the experiment, as the participant was palpating for the fistula, both the camera and the Leap recorded data. The code to analyze each trial was written in C++ on the Visual Studio 2013 IDE (version). The purpose of the software was to synchronize both visual feedback from the camera and the tracking data of the Leap Motion® sensor using the computer clock

(CPU time). As detailed in Figure 40, it is essential to synchronize both sensors in separate threads to analyze participant performance. Threading allows for instructions from the code to be operated concurrently; this ensures that the data from the Leap Motion® sensor and the images from the camera were recording simultaneously.

Figure 40. Detailed data acquisition to data analysis flow chart

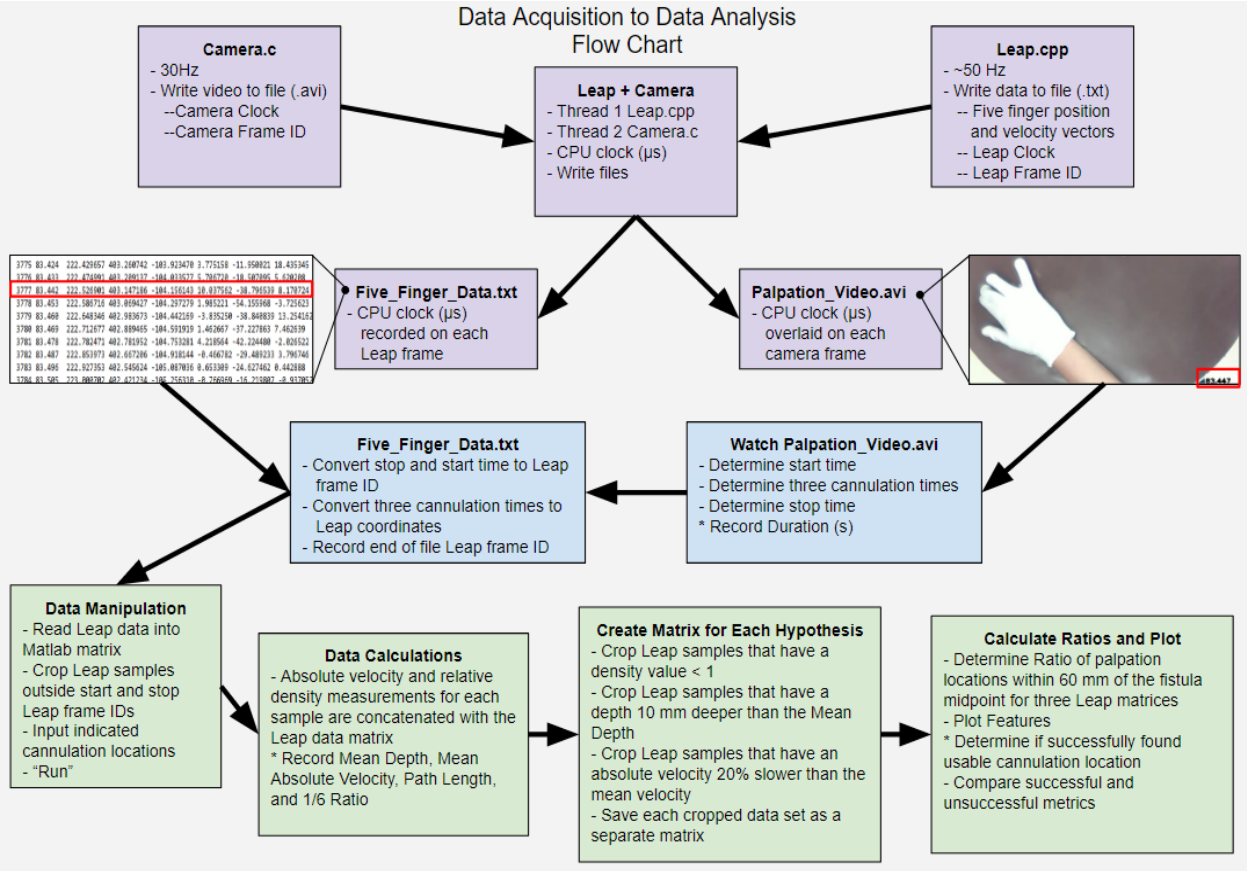

By employing threads, it is possible to use the computer's clock to accommodate for the different acquisition rates of the camera and the Leap Motion® sensor. The camera outputs a video file that is used as a reference to identify the points at which the participant indicates that they have located a viable point of needle insertion. The Leap Motion® sensor is programmed to output a text file that records the following values for each frame: the frame ID, the time, the x-coordinate

for each finger, the y-coordinate for each finger, the z-coordinate for each finger, the x-velocity for each finger, the y-velocity for each finger, and the z-velocity for each finger. These values are imported into MATLAB and are used to create new metrics that are valuable in evaluating the participant's palpation skill (Figure 40 & 41).

Figure 41. Overview of data path

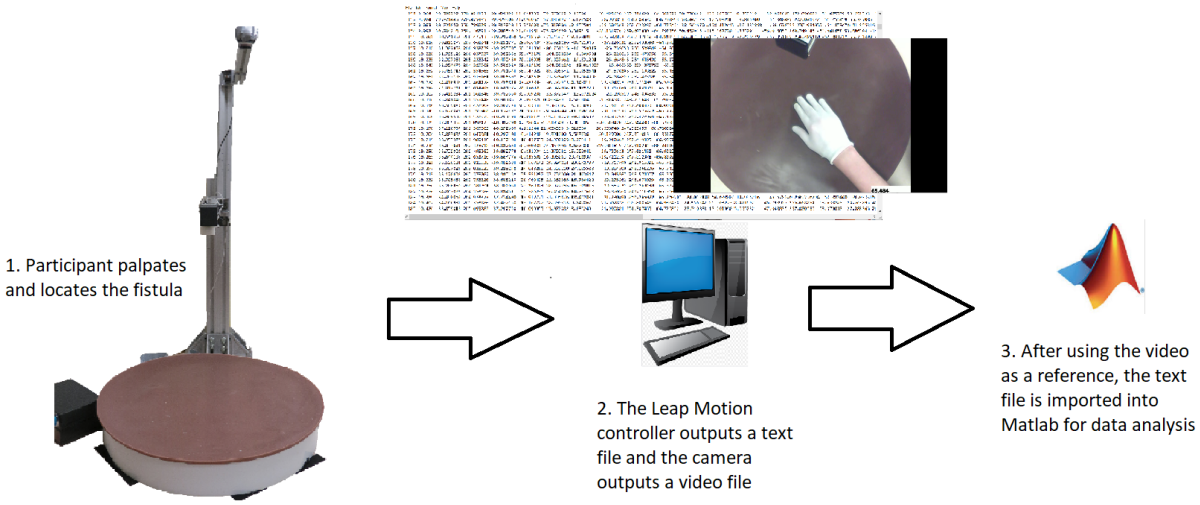

Metrics

The participant was asked to identify three points on the fistula that they determined to be proper points for cannulation. Ideally one would find the three points along the length of the

Figure 42. Ideal cannulation locations along the fistula module

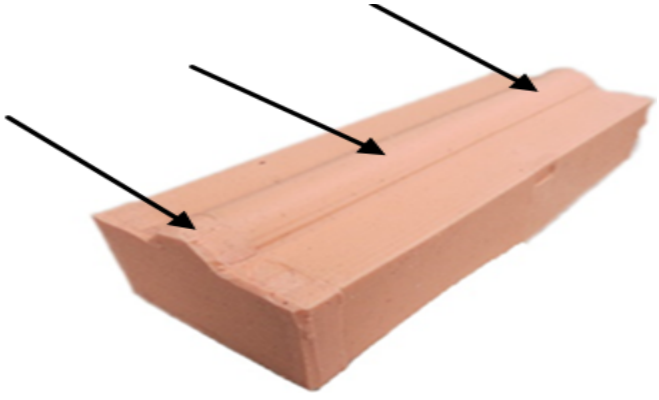

fistula as indicated in Figure 42. To classify whether the participant was successful in finding a proper cannulation location or not, the first point reported was considered as the cannulation target location. If the coordinates of the first cannulation point were determined to be in the target area (denoted by the red rectangle in Figures 51-56) then the trial was considered to be successful.

During the recorded trials, different palpation techniques were observed by participants. Some subjects used palpation techniques used by professionals, this is not surprising as most subjects had no prior experience in palpation. In order to get a sense of what techniques were used, their methods were divided into gross and fine palpation. Gross palpation was characterized as widening the palm and using the increased surface area to localize the fistula. Fine palpation was classified by clasping the fingers together to feel for more precise detail. It was expected that the participant would use gross palpation at first to determine the general direction of the fistula and then use fine palpation to meticulously pinpoint an accurate cannulation location.

The most rudimentary metric to retrieve from the experiment is the time it takes for the participant to find the fistula. To find the exact trial duration, time is calculated from when the participant moves his or her hand after having placed it upon the simulator to the time when they indicate they have found the first viable point of cannulation.

The path length metric is a scalar variable that signifies the total distance palpated by the participant to reach the first point of cannulation. This is calculated by recording the distance the index finger travels in between sequential frames and summing locations through all the frames. If the participant is not able to find a single cannulation point after moving their palm a total of 1 meter, then it is highly likely that the participant is not capable of performing the task properly.

We constructed the following hypothesis for the path length metric:

H_o: If the participant's path length is greater than the average path length and the time taken to find the fistula is less than the average time, then there is no increase in gross palpation being used.

H_a: If the participant's path length is greater than the average path length and the time taken to find the fistula is less than the average time, then there is an increase in gross palpation being used.

The palpation depth corresponds to the y-value of the index finger's coordinates. It is valuable to know where the participant is depressing into the skin during palpation; palpation at greater depths is potentially indicative of fine palpation. Fine palpation is generally used at points of interest to further analyze what the participant is feeling under the skin. During a trial the participant understands that the point of maximum vibratory stimulus is where the fistula to be found is located, so it can be hypothesized that as the participant's hand increases in proximity to the fistula, palpation depth will increase. We constructed the following hypothesis for the palpation depth metric:

H_o: When the palpation depression depth is at least 10mm deeper than the mean palpation depth, over 95% of the participant's data points are not within 60 mm of the fistula midpoint.

H_a: When the palpation depression depth is 10mm deeper than the mean palpation depth, over 95% of the participant's data points are within 60 mm of the fistula midpoint.

The palpation velocity corresponds to the magnitude of the index finger's velocity vector. Similar to the practical application of deeper palpation depressions, slower palpation velocity also is potentially indicative of fine palpation. It is important to note if the participant is slowing

their palpation speed as they are palpating in close proximity to the fistula or if they are more slowly palpating in regions away from the fistula. Should the participant palpate much slower in regions not near the fistula to be cannulated then this participant may lack palpation skill. One can hypothesize that as proximity to the fistula increases, palpation velocity should decrease due to the increased vibratory stimulus surrounding the fistula. We constructed the following hypothesis for the palpation velocity metric:

H_o: When the instantaneous palpation velocity is at least 20% slower than the mean palpation velocity, more than 95% of the participant's data points are not within 60 mm of the fistula midpoint.

H_a: When the instantaneous palpation velocity is 20% slower than the mean palpation velocity, more than 95% of the participant's data points are within 60 mm of the fistula midpoint.

Understanding the orientation of the fistula needing to be cannulated is of the utmost importance because it is easy to perforate the blood vessel if the insertion angle is incorrect. The fistula orientation value is determined by plotting the locations of the three points on the fistula that the participant is asked to identify in the x-z plane. A linear regression is then plotted between the three cannulation locations. The slope of the linear regression is the participant's orientation value for the trial. If the participant's calculated orientation value is close to the known orientation value of the fistula used, then we predict he or she has the ability to locate a viable cannulation location. We constructed the following hypothesis for the fistula orientation metric:

H_o: When the participant's slope between his or her three cannulation points and the measured slope of the fistula have less than a 10% difference, the participant's indicated point of insertion is not within the accepted area of the fistula.

H_a: When the participant's slope between his or her three cannulation points and the measured slope of the fistula have less than a 10% difference, the participant's indicated point of insertion is within the accepted area of the fistula.

The density ratio value is a metric that compares the number of data points that were harvested inside the region that housed the correct fistula in relation to the total number of data points that were collected. The six "pie" shaped regions and their corresponding boundaries can be seen best in Figure 38. The density ratio metric is valuable as it gives an approximation of whether the participant is able to quickly identify the source of the vibrating fistula. A density ratio value of over 90% indicates the participant is more likely to identify a viable cannulation point and has a degree of palpation skill. We constructed the following hypothesis for the density ratio metric:

H_o: If the density ratio between the desired 1/6 and the rest of the simulator has more than 90% of the palpation points, then the participant will not succeed in finding a fistula location to cannulate.

H_a: If the density ratio between the desired 1/6 and the rest of the simulator has more than 90% of the palpation points, then the participant will succeed in finding a fistula location to cannulate.

Further, another hypothesis can be constructed relating density ratio with time:

H_o: If the density ratio between the desired 1/6 and the rest of the simulator has more than 90% of the palpation points, then the time taken to find the fistula will not be less than the mean time spent finding the same fistula.

H_a: If the density ratio between the desired 1/6 and the rest of the simulator has more than 90% of the palpation points, then the time taken to find the fistula will be less than the mean time spent finding the same fistula.

Density is an important metric when classifying a participant's palpation skill because an elevated density value location represents where a participant spent a significant amount of time. Positional information regarding where the participant spent most of his or her time is a potential metric for how skilled at palpation the participant is. The density value is simply counting how many index finger locations are within a circle centered on each index finger's location and then divided by the area of the circle. Every index finger coordinate has a circular area around it; the density function counts how many other index finger locations are within that defined radius. For example, if the subject were to hold his or her index finger in one location for an extended period of time then a high-density value would ensue because of all the samples collected at that particular location. Further, if one were to move his or her index finger at a constant velocity in an x-shaped pattern on the surface of the simulator then the center of the x would have the highest density value because it is the only location that has a path intersection. It is, therefore, appropriate to hypothesize that high-density palpation locations will be where the participant feels something of interest under the skin. If high density locations are not found near the fistula, this is an indication of lack of palpation skill. We constructed the following hypothesis for the density metric:

H_o: Palpation locations with a density value greater than 1 will not 100% of the time be within 60mm of the fistula midpoint.

H_a: Palpation locations with a density value greater than 1 will 100% of the time be within 60mm of the fistula midpoint.

RESULTS

The following tables and graphs demonstrate behavioral differences between novices who succesfully found the fistula to those who did not.

Table 9. Meaningful features relevant to measuring palpation skill (green is a successful trial)

Trial Number	Experimental Slope	Fistula Slope	Distance between Cannulation Location and Fistula Midpoint (mm)	Angle from Cannulation Point to Fistula Midpoint (°)	Duration (s)	Path Length (mm)	Mean Depth (mm)
1	1.452	1.951	7.755	28.845	19.968	1853.500	448.926
2	0.760	1.951	68.532	-65.114	10.041	849.988	415.905
3	2.052	1.951	57.251	-54.039	5.153	224.785	406.487
4	2.585	1.951	46.047	-67.992	16.560	932.766	412.348
5	2.212	1.951	61.539	-67.918	8.538	313.069	409.423
6	1.134	1.951	71.025	-57.672	5.903	151.247	404.991
7	0.786	1.951	43.462	-62.968	40.777	245.543	398.084
8	1.611	1.951	70.010	119.314	16.186	1716.800	417.970
9	2.046	1.951	17.494	135.377	10.100	810.605	413.624
10	2.145	1.951	65.041	-58.723	14.890	598.636	409.440
11	1.463	1.951	21.691	-79.215	7.334	302.666	405.624
12	2.118	1.951	75.717	117.867	18.016	765.071	391.994
13	1.364	1.951	73.469	-75.833	17.520	259.923	414.022
14	0.423	1.951	60.403	143.785	44.418	1892.300	415.178
15	2.533	1.951	27.714	-106.670	34.827	1413.400	423.849
16	1.139	1.951	28.689	150.039	22.704	1988.100	427.763

Trial Number	Mean Velocity (mm/s)	Inside Correct 1/6 of Simulator (%)	Density>1 within 60mm of Fistula Midpoint (%)	10mm Deeper than Mean Depth within 60mm of Fistula Midpoint (%)	20% Less than Mean Velocity within 60mm of Fistula Midpoint (%)	Fine Palpation (%)	Gross Palpation (%)
1	31.977	93.990	100.000	98.040	92.030	5.600	94.400
2	50.198	82.120	0.000	0.000	0.190	0.000	100.000
3	57.949	100.000	98.300	0.000	93.600	95.000	5.000
4	85.341	76.270	73.880	50.310	64.490	23.000	77.000
5	57.943	88.260	2.350	0.000	28.310	0.000	100.000
6	40.737	97.950	0.000	0.000	0.000	6.600	93.400
7	54.230	100.000	77.920	0.000	94.080	0.000	100.000
8	67.767	69.970	18.420	0.000	25.190	75.000	25.000
9	101.785	85.390	96.550	19.460	86.270	80.000	20.000
10	79.493	96.070	15.370	0.000	15.350	97.000	3.000
11	73.829	100.000	100.000	0.000	97.830	27.800	72.200
12	70.330	93.670	68.740	68.740	68.740	72.200	27.800
13	36.949	67.790	0.000	0.000	0.000	100.000	0.000
14	68.269	32.780	36.820	26.050	22.690	100.000	0.000
15	65.639	60.750	25.150	37.880	23.470	100.000	0.000
16	121.664	94.880	66.880	42.910	57.990	66.600	33.400

Figure 43. Three indicated cannulation locations color coded by trial (all 16 trials)

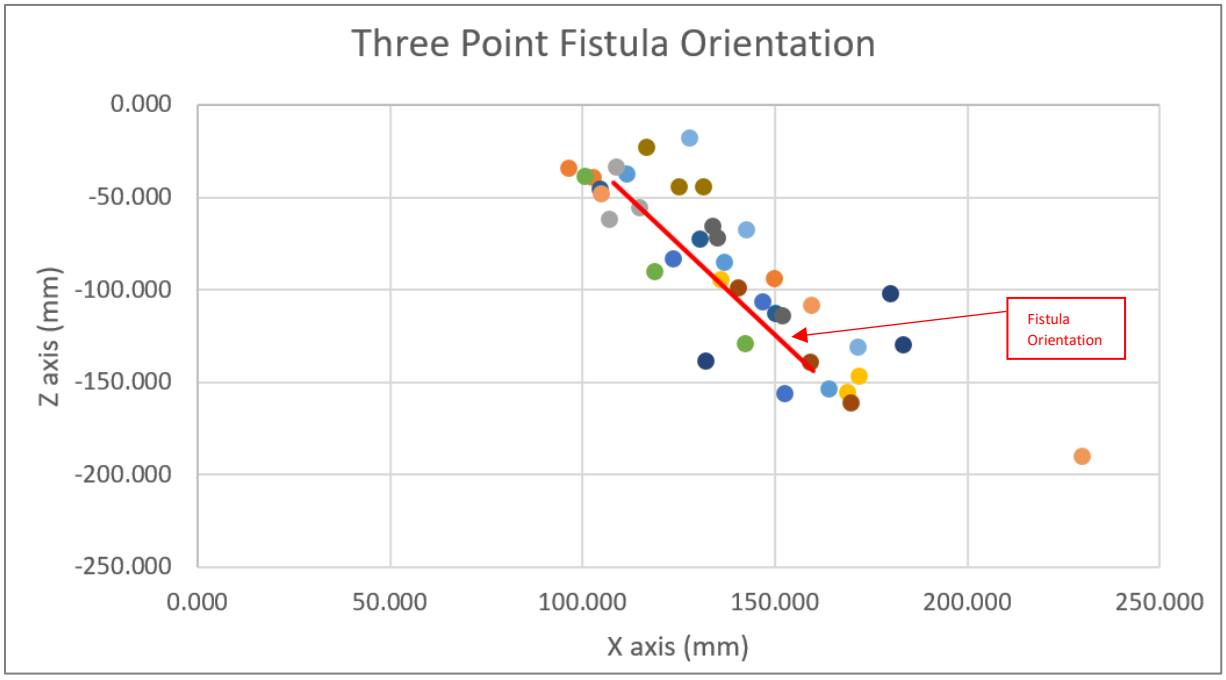

Figure 44. Slope values from the linear regression through each trial's three cannulation locations (1.95 is the actual slope of the fistula)

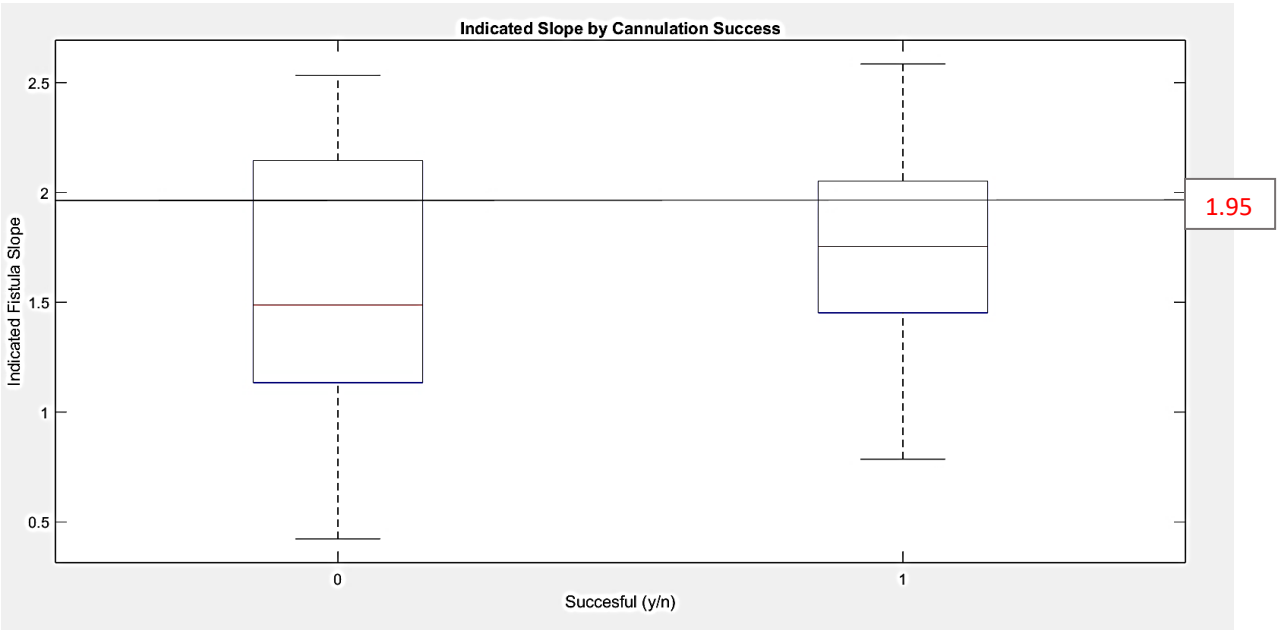

Figure 45. Distance in millimeters between indicated cannulation location and fistula midpoint

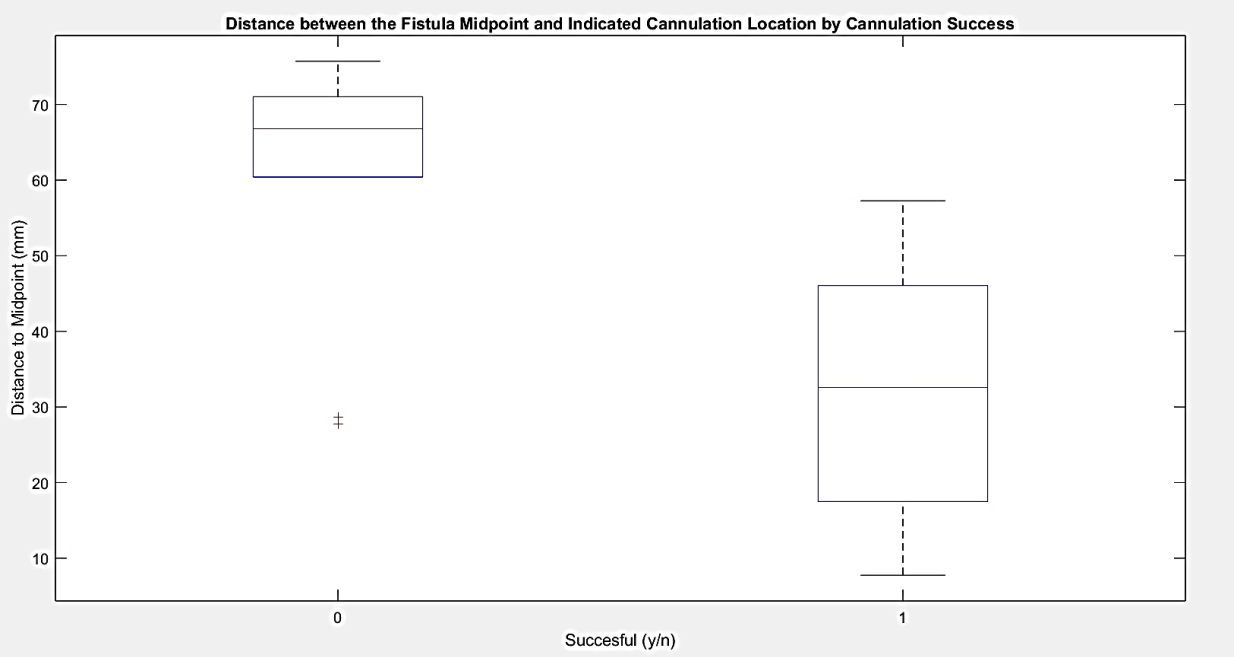

Figure 46. Angle in degrees, -180:180, from indicated cannulation location to fistula midpoint

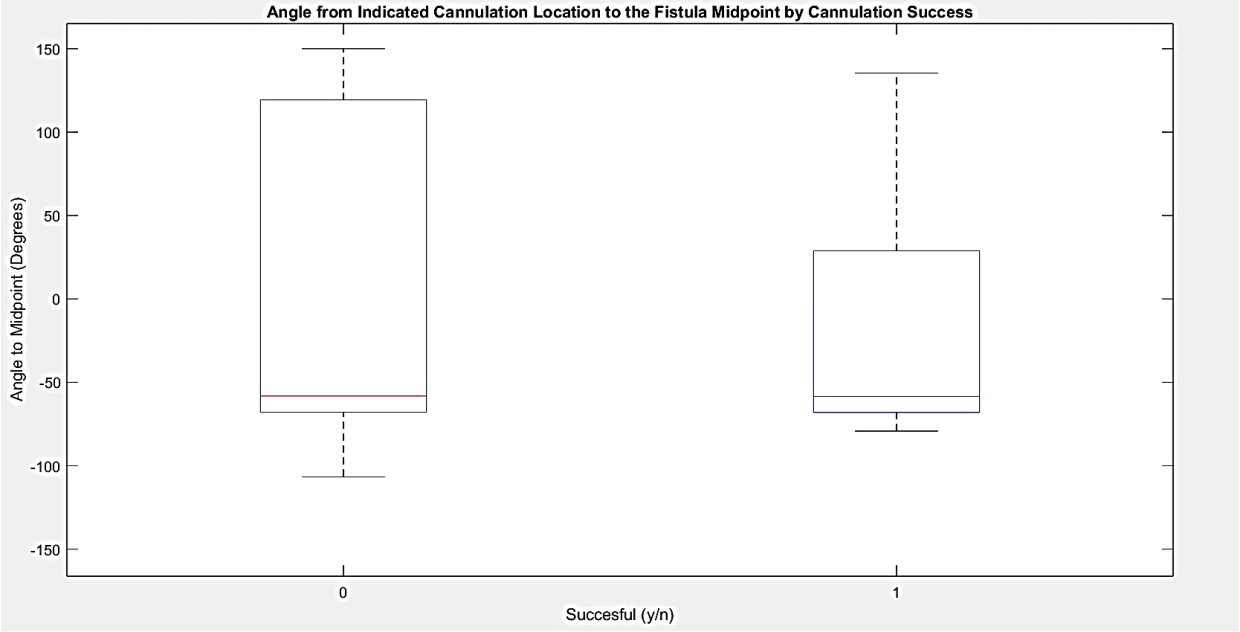

Figure 47. Time in seconds needed to find a cannulation location

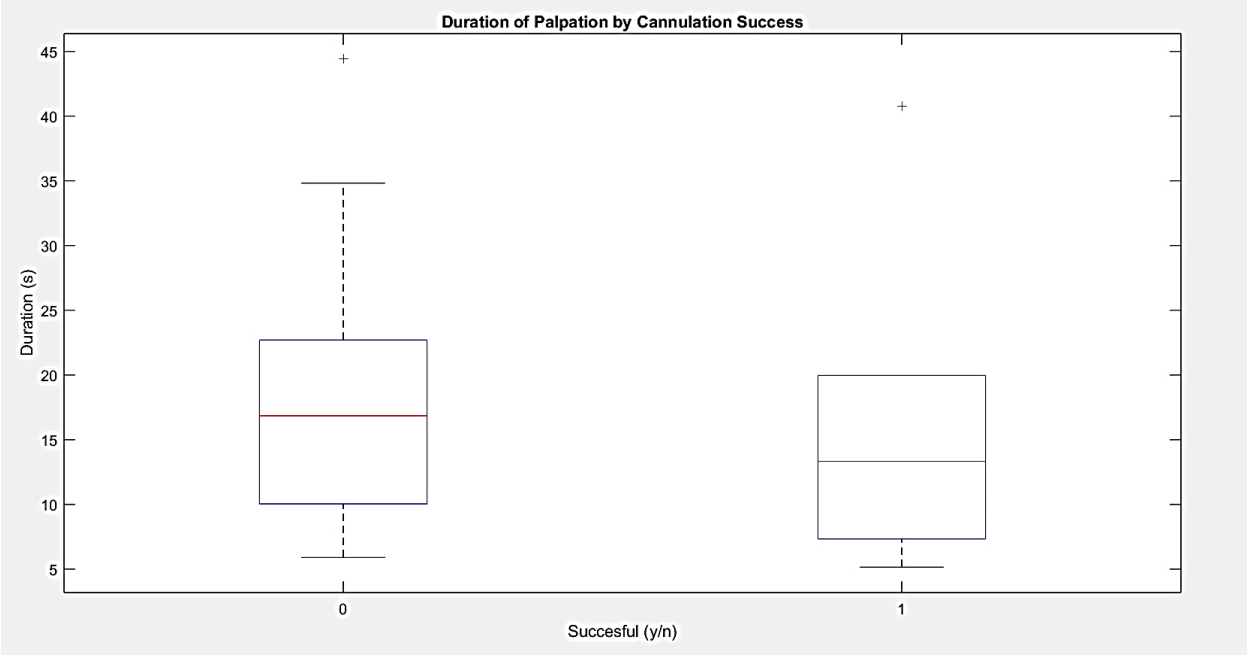

Figure 48. Palpation path length in millimeters needed to find a cannulation location

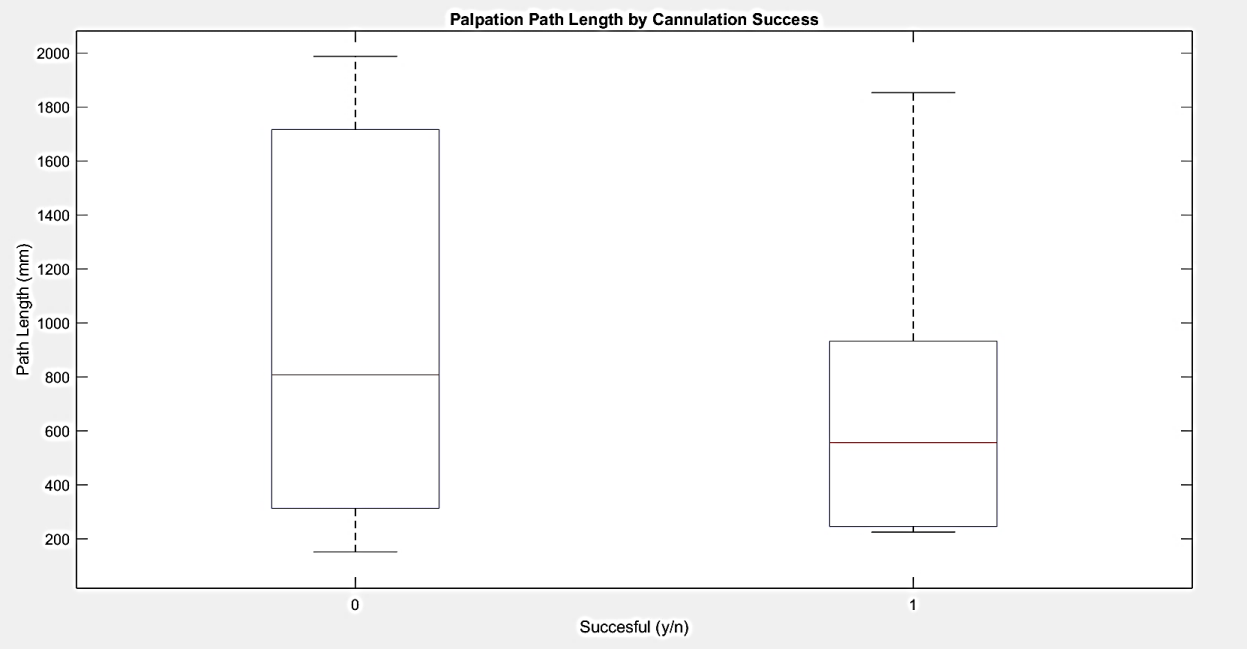

Figure 49. Percentage of palpation locations inside the correct one sixth of the simulator

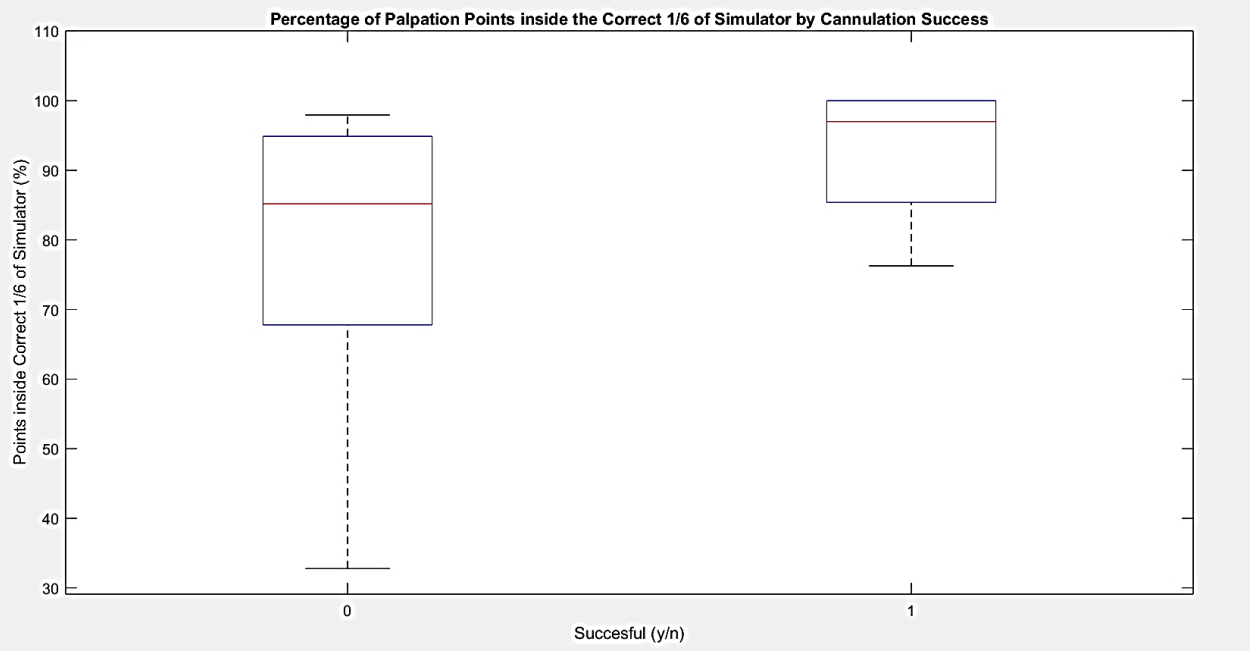

Figure 50. Proportion of gross and fine palpation used in successful vs. unsuccessful trials

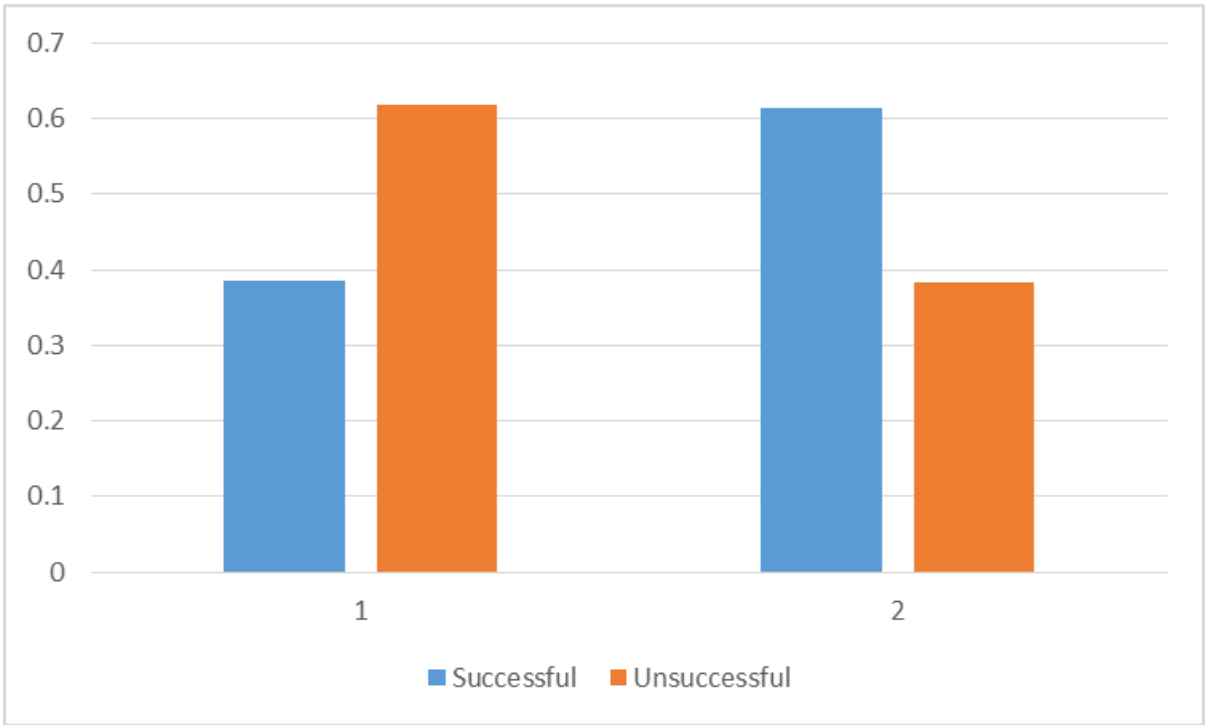

Figures 51 & 52. Index finger palpation path overlain with density topography (unsuccessful and successful examples anytime there are two figures side by side, the small black circle is the participant's indicated cannulation location)

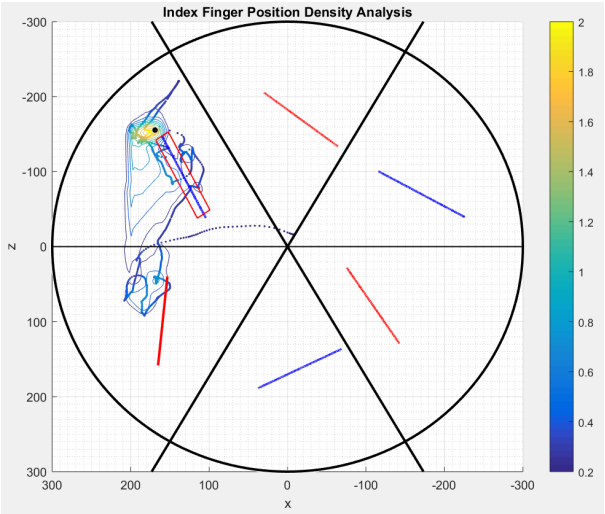

Unsuccessful Cannulation trials

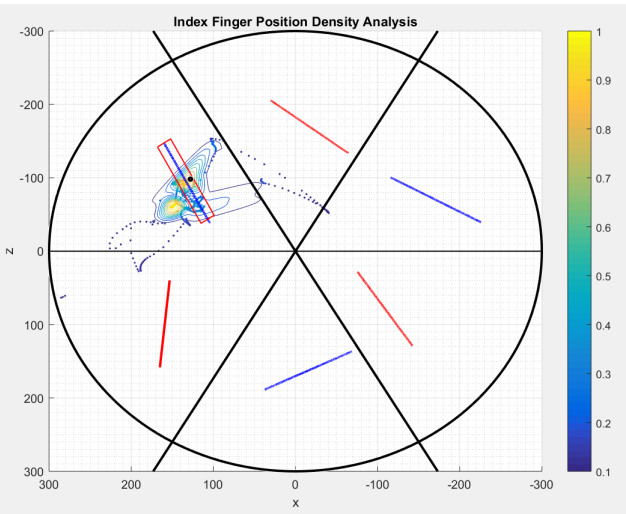

Successful Cannulation trials

Figures 53 & 54. Index finger palpation path color coded with density values

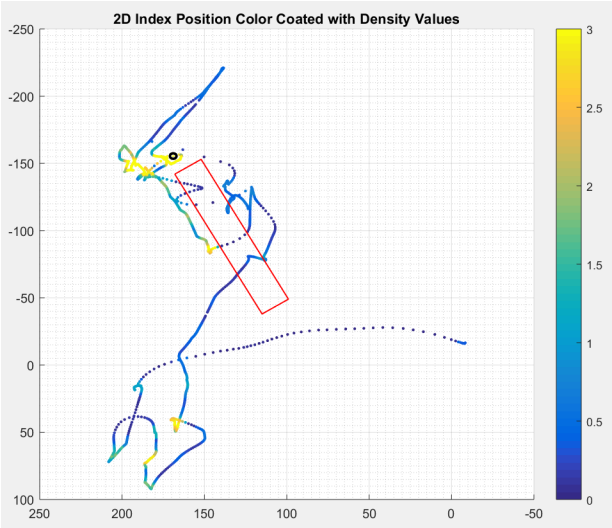

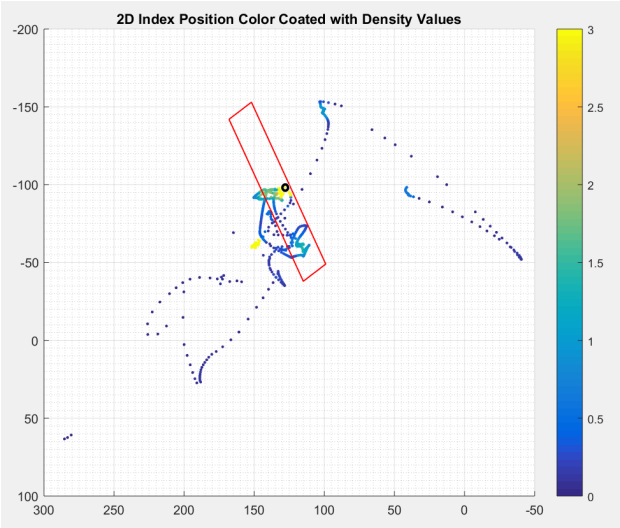

Figures 55 & 56. Index finger locations with a density value greater than 1

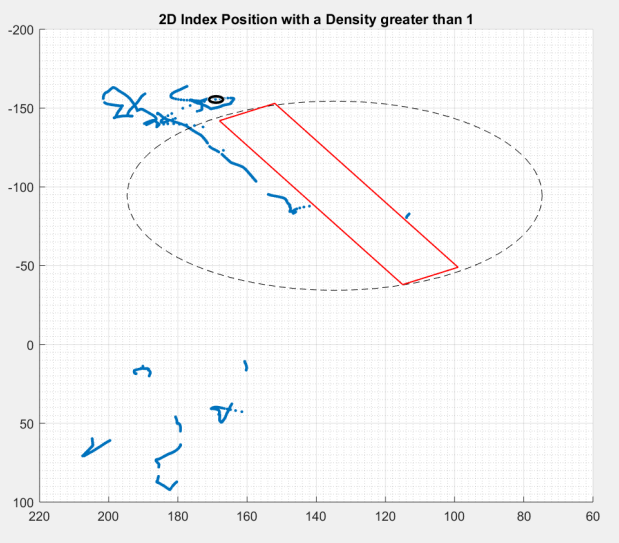

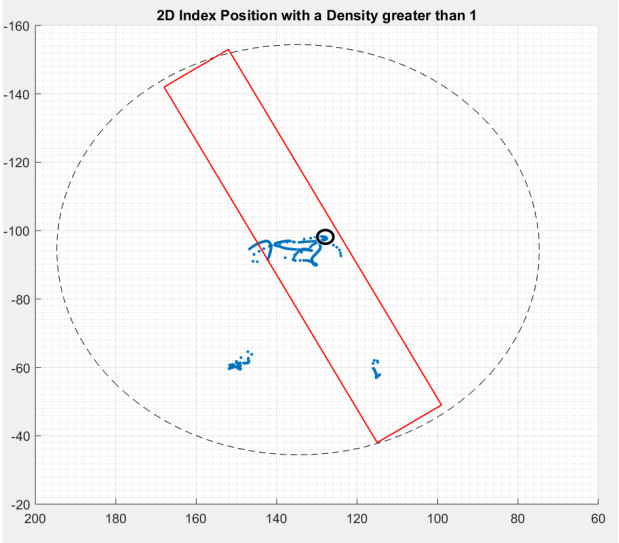

Figure 57. Percentage of palpation locations within 60 mm of the fistula midpoint that also have a density value greater than 1

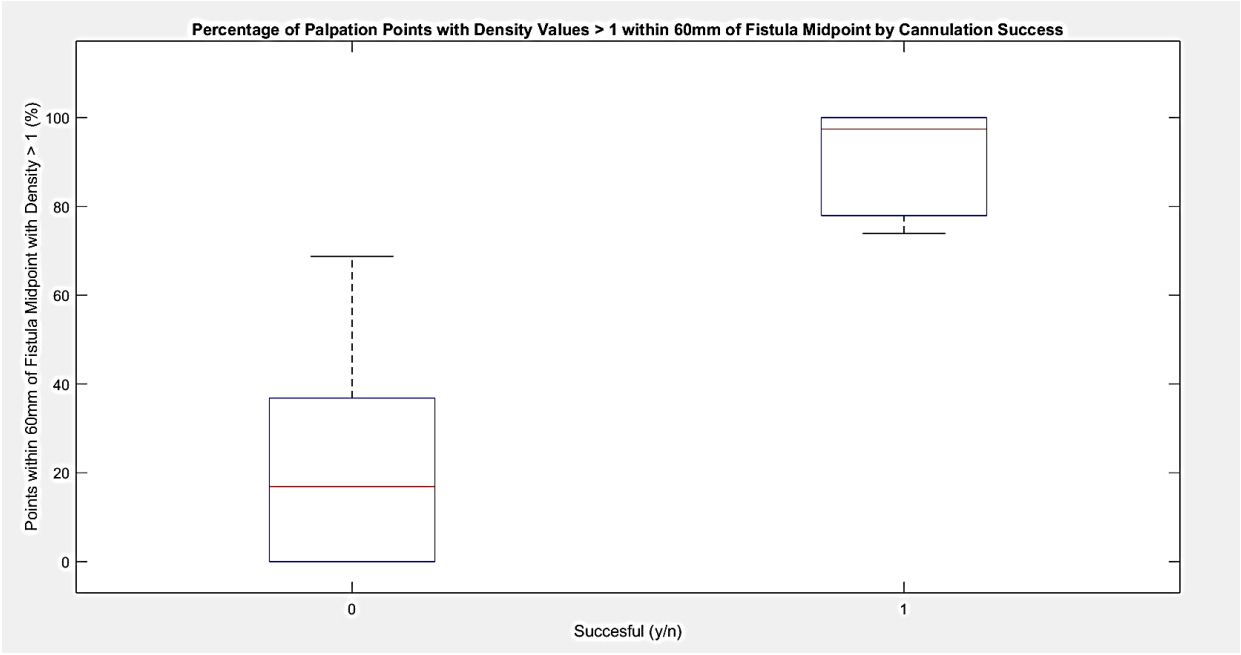

Figures 58 & 59. Index finger palpation path color coded with depth values

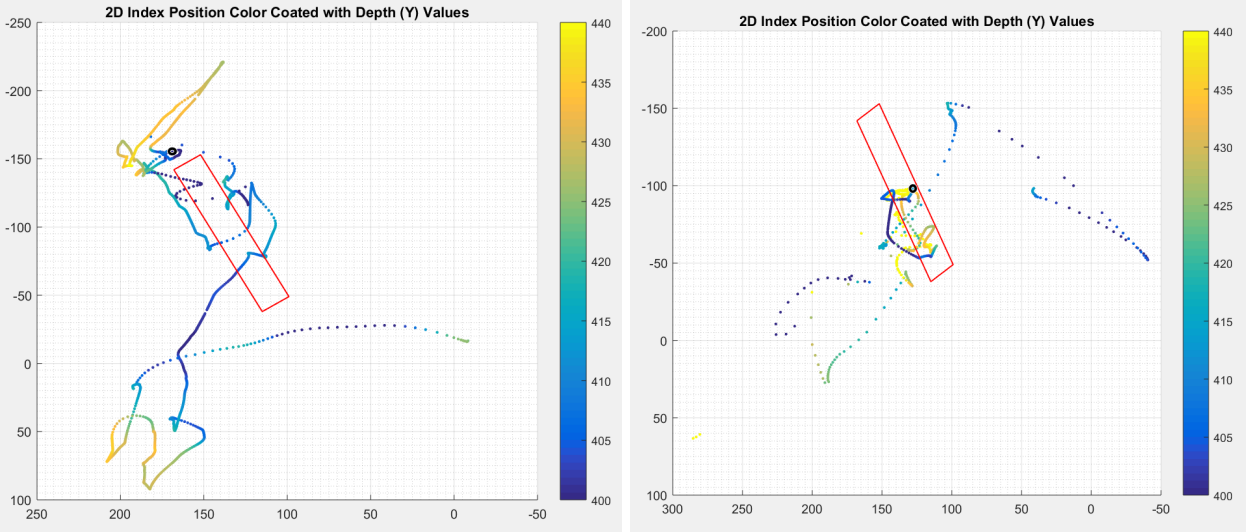

Figure 60. Mean palpation depth used to find a cannulation location

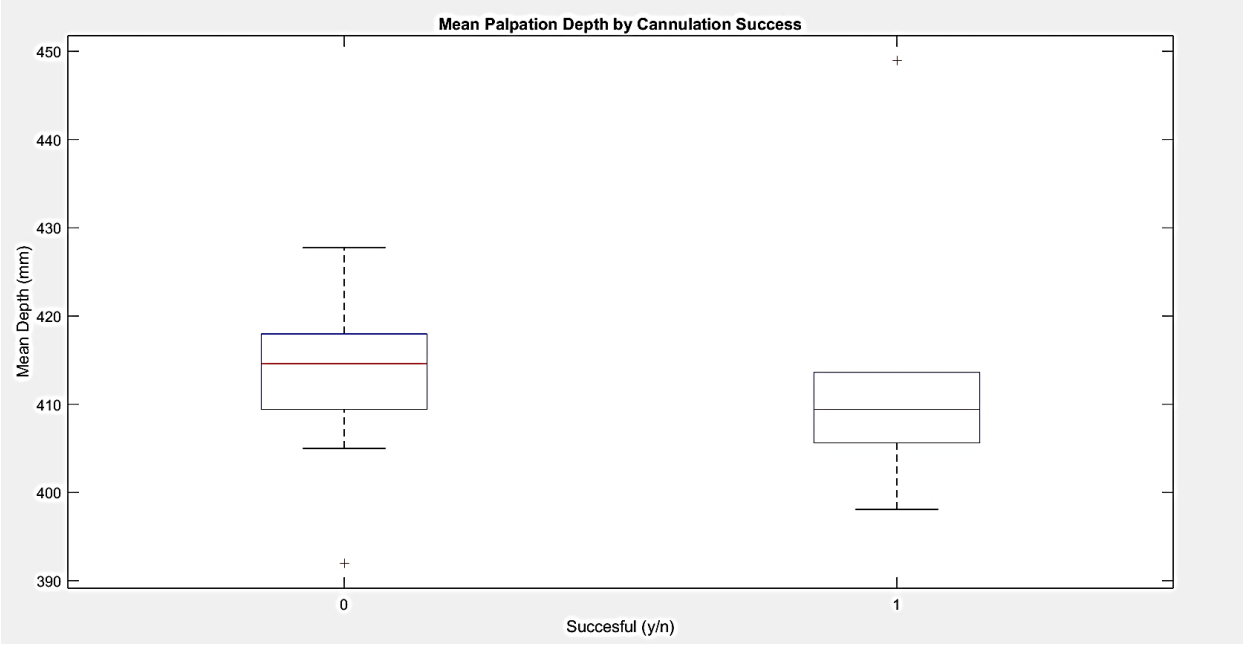

Figures 61 & 62. Index finger palpation locations with a palpation depression depth 10 mm deeper than the current trial's mean palpation depth

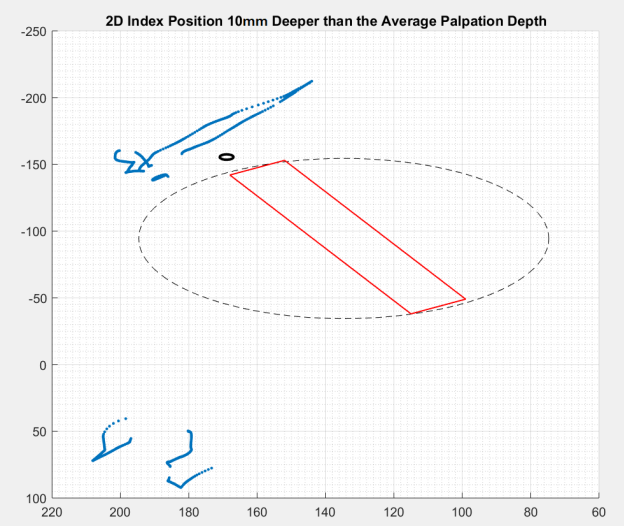

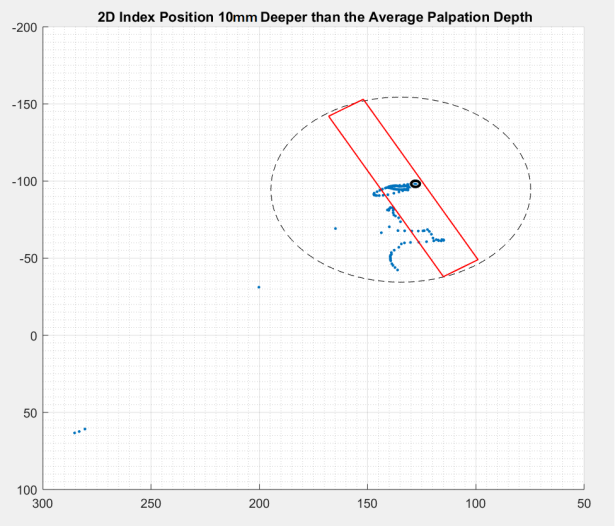

Figure 63. Percentage of palpation locations within 60 mm of the fistula midpoint that also have a palpation depth 10 mm deeper than the current trial's mean palpation depth

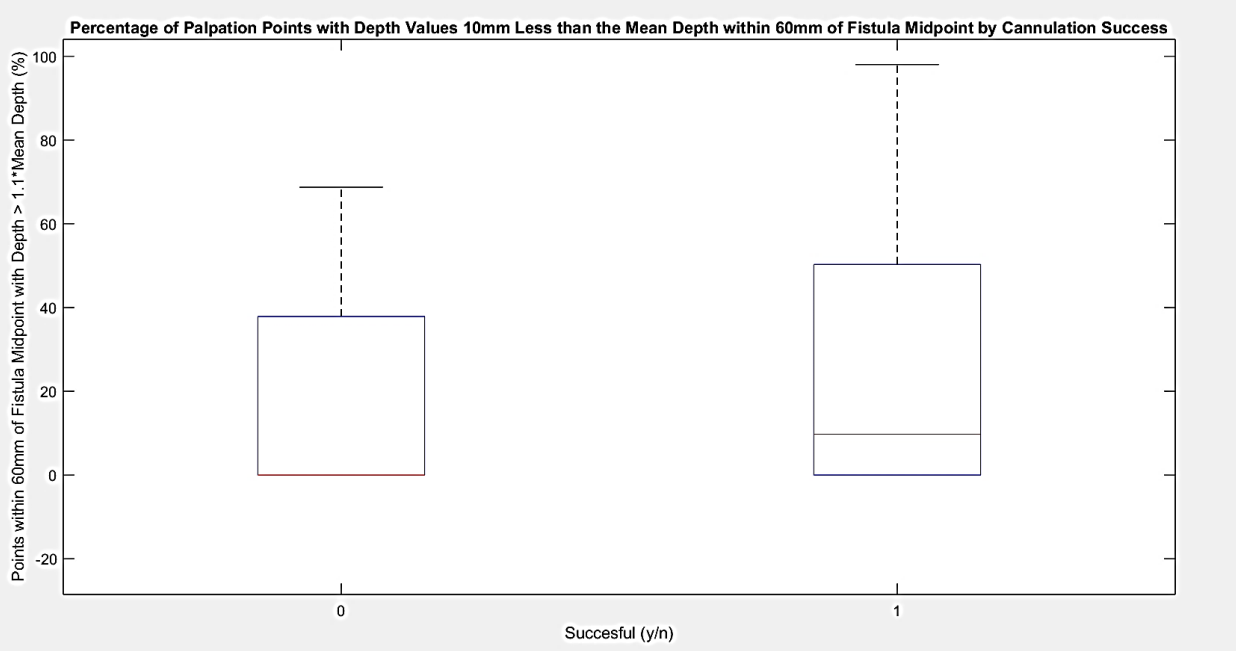

Figures 64 & 65. Index finger palpation path color coded with velocity values (mm/s)

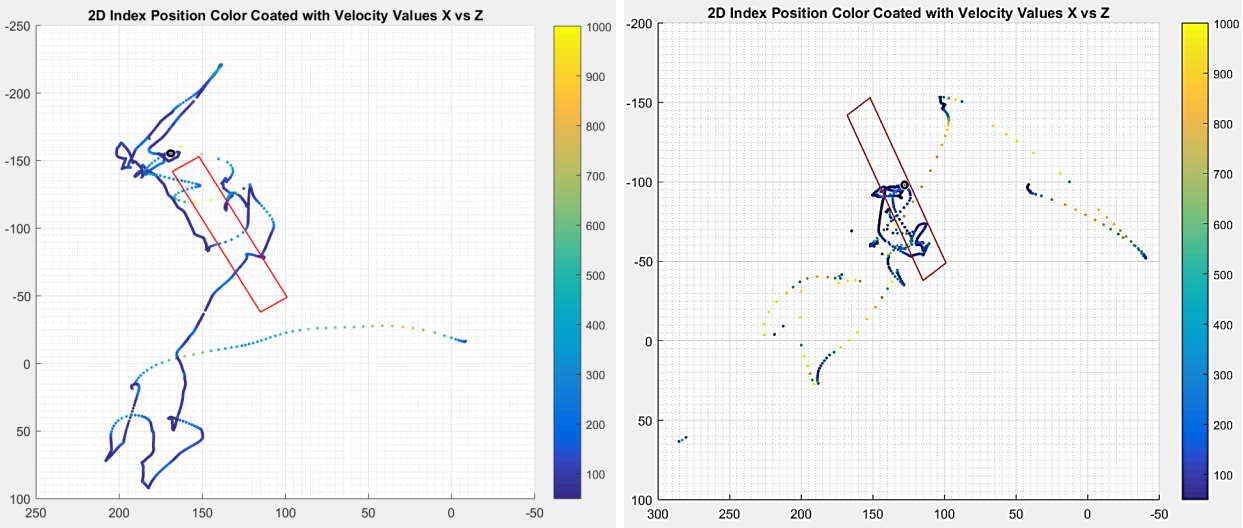

Figure 66. Mean palpation velocity in millimeters per second used to find a cannulation location

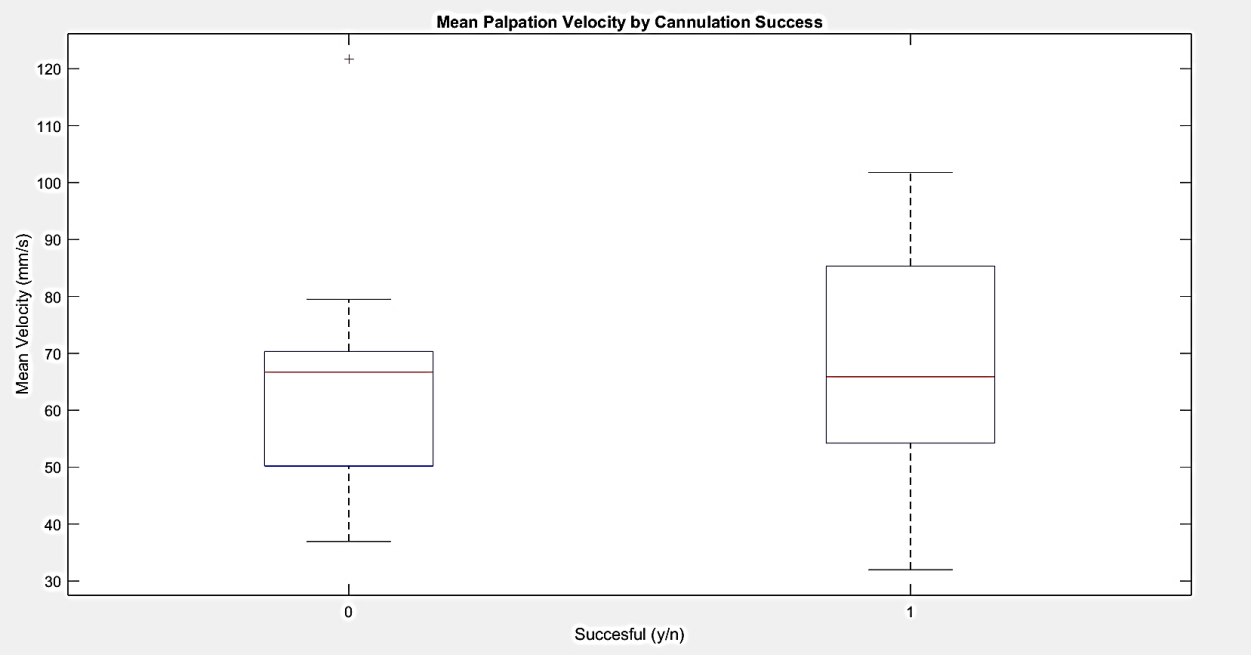

Figures 67 & 68. Index finger locations where palpation velocity is 20% slower than the current trial's mean palpation velocity

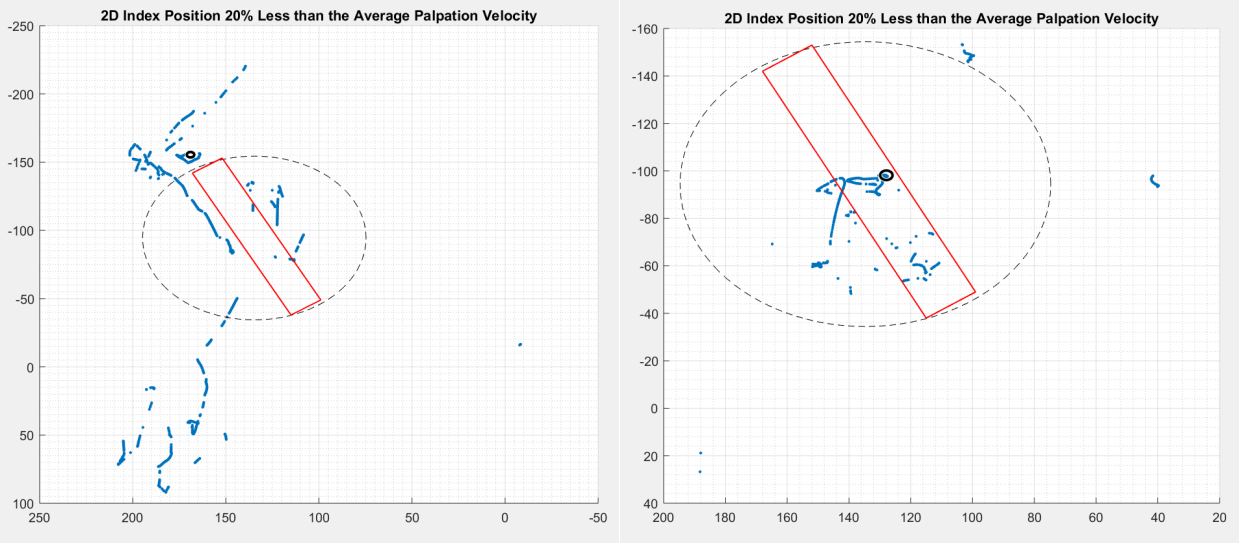

Figure 69. Percentage of palpation locations within 60 mm of the fistula midpoint that also have an instantaneous palpation velocity 20% slower than the current trial's mean palpation velocity

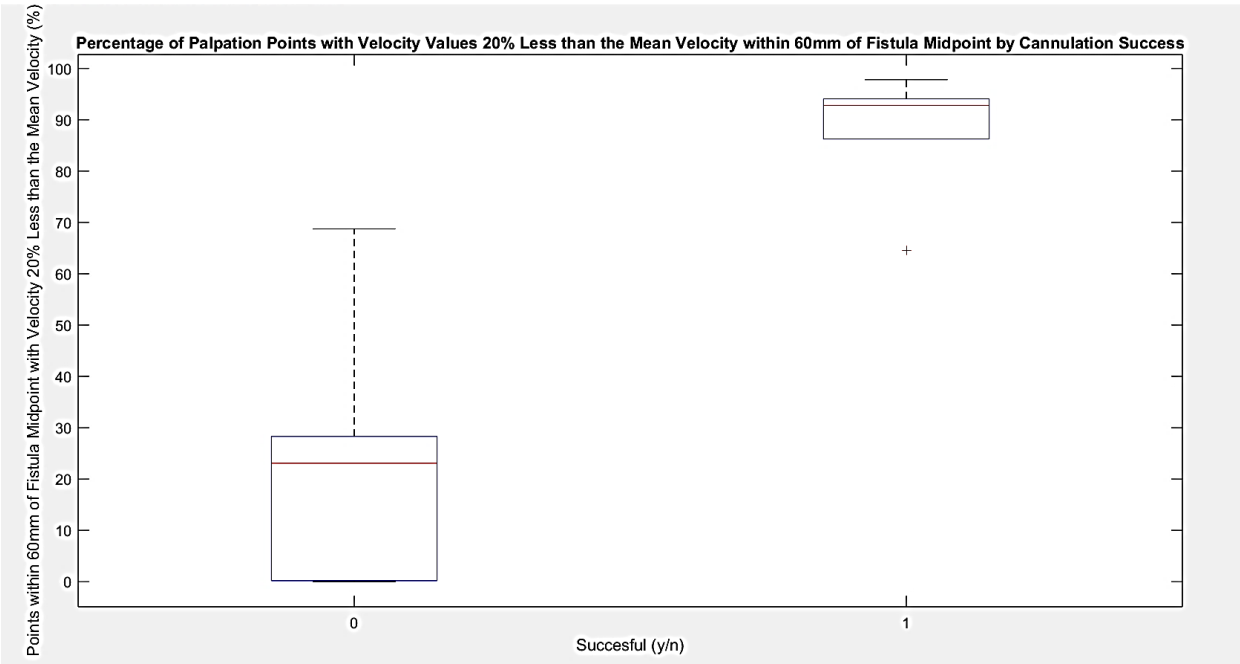

DISCUSSION & CONCLUSIONS

Palpation skill analysis is largely unprecedented aside from breast tissue examination technique. Currently there are no defined procedures for teaching how to palpate properly based on objective data. The cannulation of an AV fistula requires palpation for finding the ideal needle locations in order for dialysis treatment to proceed. In this study we have detailed a few sensor-based metrics, and collected data from novices towards preliminary results. The analysis of these preliminary results is integral for further development of the cannulation simulator since it will structure the future design of the simulator.

The first metric we will be discussing is the fistula orientation value. Figure 44 divides the sixteen trials' cannulation locations (Figure 43) into successful and unsuccessful trials. Six out of sixteen participants successfully found an acceptable cannulation location (previously defined on pg. 45). Out of those six successful trials only two orientation values were less than 10% different from the actual orientation value, 1.95. (The actual orientation value of the fistula, 1.95, was simply determined by plotting a linear regression through the three locations along the fistula indicated in Figure 42 and recording the slope of that regression.) Only one trial was successful when the participant's orientation value was more than 32% different. The mean orientation value for unsuccessful trials is 1.54 while the mean orientation value for successful trials is 1.73. It is evident that palpating to determine fistula orientation is important for finding a successful cannulation location. Should we collect more trials, we believe this trend will become even more apparent and will be deemed a useful metric for predicting cannulation success.

The distance between the participants' indicated cannulation location and the middle of the fistula can be seen in Figure 45. Successful participants on about median were 32.28 mm

away from the fistula midpoint while unsuccessful participants were on about 60.21 mm away from the fistula midpoint. Neither of these statistics are surprising because the target region on the fistula model itself is approximately 120 mm in length, so it stands to reason that any cannulation location more than 60 mm away from the fistula midpoint would be unsuccessful. Successful trials having an average of 32.28 mm distance from the fistula midpoint is not alarming because we did not ask the participants to find the midpoint of the fistula. We simply asked them to find a viable cannulation location along the 120 mm fistula vessel. One interesting observation is that two unsuccessful trials were less than 30 mm away from the fistula midpoint but failed to find a viable cannulation location.

Palpation duration when combined with other metrics can provide insight into what kind of palpation technique was used to find the fistula. Figure 47 illustrates the time taken for successful trials versus unsuccessful trials to find a cannulation location. Successful participants on average palpated for 16.65 s before finding a cannulation location while unsuccessful participants spent 19.34 s palpating for the fistula. This is not very telling without being placed in context with other metrics such as path length, ratio values, and gross and fine palpation percentages. Figure 48 demonstrates unsuccessful participants had a much greater variability in path length with an average of 994.85 mm while successful participants remained more deliberate in their palpation path with an average path length of 728.31 mm. The mean ratio of palpation locations within the correct fistula region for successful participants is an incredible 92.61 %; whereas, unsuccessful trials averaged a ratio of 78.42 % within the correct region (Figure 49). The average gross palpation used for successful participants was 61.43 % whereas the average fine palpation used for unsuccessful participants was 38.26 % (Table 9). It is important to note the ratio of fine versus gross palpation technique is almost exactly inversed for

successful versus unsuccessful participants (Figure 50). (In summary, successful participants spend less time finding a cannulation location, have a much shorter path length, palpate in the correct region of the simulator for a larger percentage of time, and use gross palpation for 2/3 of the trial.)

These trends indicate successful participants are able to localize the source of the vibratory stimulus much more rapidly than unsuccessful participants which in turn results in a decreased palpation duration time, a shorter path length, and an increased ratio of palpation locations lying within the correct 1/6 of the simulator. Successful participants used fine palpation for only 1/3 of the trial. Skilled participants require less time to find a viable cannulation location once they have arrived at the vibrating fistula; therefore, it stands to reason that they are more skilled in localizing the source of the vibratory stimulus, which results in less time spent utilizing fine palpation. It also stands to reason that if unsuccessful participants lack skill in localizing the vibrating fistula then they will use a much larger percentage of fine palpation to verify whether they have or have not found the vibrating fistula beneath the simulator's skin.

It was noted that eleven participants had a trial duration time shorter than the mean, 18.31 s, and that six participants had a palpation path length longer than the mean, 894.90 mm. Three out of the ten and two of the six participants were able to successfully find a viable cannulation location. Only one participant had a shorter trial duration than the mean and had a longer path length than the mean. One participant was an outlier for our hypothesis that there would be a substantial increase in gross palpation should both of these conditions be met. In fact, the exact opposite proved to be true; the participant used 75% fine palpation to find a cannulation location.

We also hypothesized that if the ratio between the desired 1/6 and the rest of the simulator has more than 90 % of the palpation locations, then the participant will succeed in

finding a viable cannulation location. Results demonstrated that out of the six participants who found a viable cannulation location, four participants had a ratio greater than 90 %. Exactly half of the participants had a ratio greater than 90 %. These results incline us to believe this hypothesis will hold true should we take more trials. In parallel to the previous ratio hypothesis, we predict that if the ratio is greater than 90 % then the trial duration will be less than the mean trial duration. As stated before, eight participants had a ratio greater than 90 %, five of which also had a trial duration time less than the mean. Both of these hypotheses essentially mean that if the participant is primarily palpating in close proximity to the vibrating fistula without wandering about the simulator then the trial will be a success. Therefore, density ratio is a key metric for measuring palpation skill.

Density of palpation locations appeared to be a promising metric for quantifying locations of interest on the simulator. Figures 51, 53, and 55 are for one unsuccessful participant; Figures 52, 54, and 56 are for one successful participant. Figures 51 and 52 provide an illustration of the path the participant took to find their cannulation location (small black circle) with respect to the simulator as a whole. The palpation path itself is color coded with density values, blue being low density, and superimposed is the density topography which is also color coded with density values. The yellow hotspots are locations where the participant palpated the most and are, therefore, areas of high interest for analysis. Zoom fitting Figures 51 and 52 to the locations where each participant palpated on the simulator and removing the density topography leaves us with Figures 53 and 54. It is much easier to discern the exact location where the palpation density is high and low with the zoomed in path plots. Of particular interest is that the successful participant's highest density locations lie along the fistula (red rectangle), but the unsuccessful participant has multiple high-density locations not along the fistula.

We propose that high density locations not in close proximity to the fistula indicate a lack of palpation skill. Figures 55 and 56 further amplify this prediction by only plotting palpation path locations that have a density value greater than 1. (A density value greater than 1 means there are at least 78 palpation locations within 5 mm of a given coordinate along the palpation path.) As a start our hypothesis to test our prediction is that palpation locations with a density value greater than 1 will always be within 60 mm of the fistula midpoint. The dotted gray circle encompassing the fistula represents the 60 mm radius circle which we initially believed to be an accurate representation of the extent of the fistula's vibratory stimulus. It can be clearly seen that 100 % of the successful participant's palpation locations with an associated density value greater than 1 are well within 60 mm of the fistula midpoint. In contrast, the unsuccessful participant has less than 50 % of palpation locations with an associated density value greater than 1 within 60 mm of the fistula midpoint. These results validate our hypothesis. Figure 57 demonstrates the trend in density values. Successful participants had density values greater than 1 within 60 mm of the fistula midpoint on average 91.11 % of the time. Unsuccessful participants had density values greater than 1 within 60 mm of the fistula midpoint on average 23.37 % of the time. After we take more trials, if we are able to able to further prove this hypothesis then one can subsume that density values greater than 1 not in close proximity to the fistula are an indication the participant lacks palpation skill.

Palpation depth is the next metric we believed could have an interesting correlation with palpation skill. Figures 58, 61 and 59, 62 are respectively plots of the same unsuccessful and successful participants we just performed density analysis on in the previous Figures. Figures 58 and 59 illustrate the palpation path color coded with depth values, bright yellow being the deepest depressions. It can be clearly seen in Figure 59 that the successful participant's deepest

palpation depressions are within close proximity to the fistula; whereas, the unsuccessful participant in Figure 58 has multiple deep palpation depressions not adjacent to the fistula. These results were expected because it was predicted that skilled participants would utilize palpation techniques that required variable force to discern what they are feeling through the skin when they encounter a vibratory stimulus or obstruction. In an article detailing the manual palpation of hard nodules in soft tissues, it was observed that in order to examine a soft environment and discover the random hard insertions in an "efficient" manner the participant applies variable examination techniques utilizing force modulation. After a hard nodule was discovered within the soft tissue, a decrease in stress magnitude was observed.[8] There is a positive correlation between palpation depression depth, applied force, and stress magnitude. We did observe that the mean palpation depth of successful participants, 407.23 mm, was less than that of the unsuccessful participants, 415.39 (Figure 60). We did not observe a reduction in palpation depth once the participant began palpating over the fistula; ergo, we did not observe a reduction in applied pressure once the participants located the fistula.[8] We hypothesized 95 % of palpation locations with a depression depth 10 mm below the current trials mean palpation depth would be within 60 mm of the fistula midpoint. Figures 61 and 62 support this hypothesis; they demonstrate that unlike in unsuccessful trials, successful participants begin to depress deeper into the simulator as they feel increasing vibratory stimulus and something stiff beneath the skin. Figure 63 shows that this trend only very mildly holds true. Successful participants had an average of 13.95 % of their 10 mm deeper palpation locations within 60 mm of the fistula, and unsuccessful participants had an average of 11.87 %. While these results are inconclusive and do not coincide with our hypothesis, we believe that our sample population skews our results because none of them have prior palpation experience and therefore cannot be held accountable

for not using variable pressure techniques. Our results do match that of previous studies which specify that applied palpation force is statistically insignificant on the rate of hard nodule detection.[8] For future studies it will be necessary to record trials using experts and novices in order to rule in favor or rule out palpation depression as a metric of skill. It should be noted that depression may be better measured with a force sensor.

Our next metric, palpation velocity, it has been observed that experts utilize force and velocity modulation to locate hard inclusions, though for novices only palpation velocity modulation influences the degree of detection.[8] Palpation velocity is believed to be a key metric in measuring the skill of the participant. The highest detection rate for discovering hard nodules in soft tissue is observed for "slow palpation velocity."[8] Figures 64 and 65 are plots of the index finger's palpation path color coded in velocity values (mm/s), blue being the slowest. The unsuccessful participant, Figure 64, is palpating relatively slow during the entire trial, but the successful participant, Figure 65, palpates quickly away from the fistula and much more slowly when in close proximity to the fistula. The mean palpation velocity for unsuccessful participants was 65.90 mm/s and for successful participants it was 67.52 mm/s (Figure 66). We hypothesize all palpation locations with palpation velocities 20 % slower than the current trial's mean palpation velocity will be within 60 mm of the fistula midpoint. It is observed in Figures 67 and 68 that the unsuccessful participant has a plethora of palpation locations with a 20 % decrease in velocity away from the fistula; however, the successful participant has the vast majority of his decreased velocity locations in close proximity to the fistula. These findings are further supported by Figure 69 where it is made very obvious that successful and unsuccessful participants use very different velocity modulation techniques. Unsuccessful participants on average only had 24.19 % of their 20 % slower palpation locations within 60 mm of the fistula

midpoint. In contrast, successful participants had an incredible 88.05 % of their 20 % slower velocity palpation locations within 60 mm of the fistula midpoint. These results support our hypothesis, and we expect this trend to continue should we take more trials in the future. Decreased velocity in close proximity to the fistula is a useful metric for measuring palpation skill.

It was previously mentioned that we initially believed a 60 mm radius circle originating from the fistula midpoint to be an accurate representation of the dispersion of the fistula's vibratory stimulus. The vibration stimulus, however, was not a single motor at the fistula midpoint but, in fact, there was a vibration motor at each endpoint of the fistula. For future analysis we believe two 30 mm radius circles originating from each of the fistula endpoints to be a more accurate representation of the vibratory propagation through the simulator. We believe this will make future analysis more accurate.

In conclusion, the Leap Motion® Controller has proven to be sufficiently accurate for the analysis of palpation within the dimensions of our simulator. We have found novel metrics for measuring palpation skill and upheld some older metrics that are indicative of proper palpation technique. Palpation velocity, density, ratio of palpation location, fistula orientation, and percentage of gross versus fine palpation all are metrics that have shown trends in measuring palpation skill. For future studies, changing our sample population to a mix of experts and novices will be imperative for further discerning which metrics ought to be given the most weight. The automatic classification of palpation technique via the Leap Motion® data is the next step for enriching our study. Palpation is used in most dialysis clinics and the need to detail a standard palpation protocol for which the clinicians to expand upon is of the utmost importance for improving quality of care in the field of hemodialysis.

REFERENCES

[1] "Statistics." *Statistics | The Kidney Project | UCSF*, pharm.ucsf.edu/kidney/need/statistics.

[2] "The Basic Assessment of an AV Fistula." *AV Fistula Assessment*, www.nrsg101.com/av-fistula.html.

[3] "Hemodialysis Compared to Peritoneal Dialysis." *WebMD*, WebMD, www.webmd.com/a-to-z-guides/tc/hemodialysis-compared-to-peritoneal-dialysis-topic-overview.

[4] "Kidney Disease Statistics for the United States." *National Institute of Diabetes and Digestive and Kidney Diseases*, U.S. Department of Health and Human Services, 1 Dec. 2016, www.niddk.nih.gov/health-information/health-statistics/kidney-disease.

[5] "Hemodialysis." *National Institute of Diabetes and Digestive and Kidney Diseases*, U.S. Department of Health and Human Services, 1 Sept. 2016, www.niddk.nih.gov/health-information/kidney-disease/kidney-failure/hemodialysis.

[6] *HP Pro Webcam - Product Specifications* , support.hp.com/us-en/document/c02562529

[7] "Leap Motion®." *Leap Motion®*, www.leapmotion.com/.

[8] Konstantinova, Jelizaveta. "Behavioral Characteristics of Manual Palpation to Localize Hard Nodules in Soft Tissues." *IEEE*, vol. 61, no. 6, June 2014, pp. 1651–1659.